NASA TECHNICAL NOTE

NASA TN D-2997

NASA TN D-2997

TEST-STAND STUDY OF A VEHICLE UPPER STAGE EMPLOYING A ROTATING-SOLID-ROCKET ATTITUDE CONTROL SYSTEM AND A COMPARISON WITH ANALOG STUDIES

by A. Thomas Young and Robert L. James, Jr.

Langley Research Center
Langley Station, Hampton, Va.

NATIONAL AERONAUTICS AND SPACE ADMINISTRATION • WASHINGTON, D. C. • OCTOBER 1965

NASA TN D-2997

TEST-STAND STUDY OF A VEHICLE UPPER STAGE EMPLOYING A ROTATING-SOLID-ROCKET ATTITUDE CONTROL SYSTEM AND A COMPARISON WITH ANALOG STUDIES

By A. Thomas Young and Robert L. James, Jr.

Langley Research Center
Langley Station, Hampton, Va.

NATIONAL AERONAUTICS AND SPACE ADMINISTRATION

For sale by the Clearinghouse for Federal Scientific and Technical Information
Springfield, Virginia 22151 – Price $2.00

TEST-STAND STUDY OF A VEHICLE UPPER STAGE EMPLOYING A ROTATING-SOLID-ROCKET ATTITUDE CONTROL SYSTEM AND A COMPARISON WITH ANALOG STUDIES

By A. Thomas Young and Robert L. James, Jr.
Langley Research Center

SUMMARY

A dynamic-test-stand investigation in three degrees of rotational freedom of a space-vehicle upper stage employing a rotating-solid-rocket attitude control system is described. Experimental data received from an onboard telemetry system and a unique photographic technique are presented and compared with results obtained from an analog simulation of the dynamical system. Analysis and comparison of the results from the various sources showed that the system performed as predicted by the analog simulation, thus validating this mathematical representation of the dynamical system. It is shown that the telemetry results, although limited in accuracy, are very valuable in analyzing the attitude control characteristics of the space-vehicle upper stage.

INTRODUCTION

The rotating-solid-rocket control system which is the subject of investigation in the present report has certain attractive features which more conventional spacecraft control systems do not possess. Jet vanes, jetavators, movable main rocket nozzles, and secondary fluid injection systems must be developed as an integral part of the main rocket. However, because of the size and complexity of most propulsion systems, it is desirable to have a control system which can be independently developed. The present system which utilizes four auxiliary rockets for control forces can be developed independently of the main rocket, and in addition, it is inherently capable of providing velocity control, retrothrust, and spin-up forces. This control concept was developed under NASA contract for the George C. Marshall Space Flight Center (see ref. 1), and the Langley Research Center is conducting a comprehensive investigation of this promising control-system concept.

An analog study of the application of this system to control the attitude of a space-vehicle upper stage is presented in reference 2. In this analog analysis, mathematical expressions were used to represent the physical systems comprising the space-vehicle upper stage. The present investigation was undertaken to determine the adequacy of this analog representation of the space-vehicle upper stage.

A full-scale model of the space-vehicle upper stage which included the electro-mechanical flight systems was mounted in a dynamic test stand which provided three degrees of rotational freedom. The attitude control system was activated and provided control during programed vehicle maneuvers and disturbances imparted to the vehicle by solid-fuel disturbance rockets. Data received from an onboard telemetry system provided information on control-rocket deflections and guidance signals from attitude and rate gyros. In addition, the control-rocket thrust performance was monitored with the use of pressure transducers. A unique camera technique was employed to obtain the Euler angles which defined the vehicle attitude during the dynamic test. The data obtained from this experiment were compared with the results obtained from an analog simulation of the dynamic model in order to evaluate the adequacy of the mathematical analysis, and these comparisons are reported herein.

SYMBOLS

A,B,C	triangle defined by pivot point of dynamic model, position-indicating ball, and camera
e	distance between graduated framework and position-indicating ball when dynamic model is vertical, in.
F	thrust of one control rocket multiplied by cos 10° (control rocket cant angle), lb
h	distance between camera and graduated framework, in.
I_X, I_Y, I_Z	mass moment of inertia about X-, Y-, and Z-axes, respectively, slug-ft^2
M_X, M_Y, M_Z	disturbance moments about X-, Y-, and Z-axes, respectively, ft-lb
O	origin of X_E-, Y_E-, and Z_E-axis system
P	projection of position-indicating ball into Y_E, Z_E plane
p	rolling velocity, deg/sec or rad/sec
q	pitching velocity, deg/sec or rad/sec
r	yawing velocity, deg/sec or rad/sec
r_m	distance between pivot point of dynamic model and position-indicating ball, in.
t	time, sec
X,Y,Z	body axes of dynamic model

X_E, Y_E, Z_E	earth-fixed axes
x_E, y_E, z_E	distance along earth-fixed axes, in.
X_R, Y_R, Z_R	reference axes
x_{cr}	center of rotation from nose, ft
x_p	moment arm for control moment about X-axis, ft
x_q	moment arm for control moment about Y-axis, ft
x_r	moment arm for control moment about Z-axis, ft
α, β, ω	angles contained in triangle defined by A, B, and C, deg
δ	control-rocket deflection angle, deg
η	angle between camera line of sight and longitudinal axis of dynamic model, deg
θ, ψ, ϕ	pitch, yaw, and roll Euler angles of dynamic model relative to earth-fixed axes, deg
θ_R, ψ_R, ϕ_R	pitch, yaw, and roll reference angles relative to earth-fixed axes, deg
$\theta_\epsilon, \psi_\epsilon, \phi_\epsilon$	pitch, yaw, and roll attitude error angles relative to reference axes, deg

Subscript:

o	initial value

Dots over symbols denote differentiation with respect to time. Primes indicate uncorrected photographic data. The numbers 1, 2, 3, and 4 denote the four control rockets as shown in the following sketch (view looking forward along the X-axis):

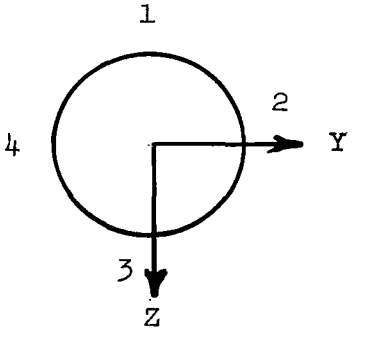

MODEL AND TEST APPARATUS

General

A dynamic model consisting of a spacecraft and ballast was used in the test-stand investigation to simulate a typical space-vehicle upper stage. (See fig. 1.) The spacecraft housed the control system of research interest, a guidance system, a telemetry system, and other supporting units. A detailed description of the guidance and control systems is given in reference 2. The ballast was employed to provide a dynamic model with center-of-gravity and inertia characteristics that approximately represented the space-vehicle upper stage used as a test bed in reference 2. The study was conducted with the use of a dynamic test stand (see fig. 1) that allowed three degrees of rotational freedom. The test setup consisted of the dynamic model mounted on a hydraulic bearing pivot allowing three degrees of rotational freedom relative to and within the bounds defined by the fixed test-stand structure. The desired test data were obtained by the telemetry system and a unique camera technique.

Dynamic Model

A sketch of the dynamic model and fixed test-stand structure is included in figure 2, and a block diagram showing the integration of the individual systems that form the dynamic model is given in figure 3.

The point of rotational freedom was located at station 132 inches which was also the approximate location of the center of gravity of the dynamic model. This geometric arrangement was accomplished by adding an additional constraint on the ballast mass and position selection. The criterion for the ballast design was to satisfy the center-of-gravity requirement as well as to produce pitch and yaw inertias similar to those of the space-vehicle upper stage.

The pitch and yaw inertias were each 1065 slug-ft^2, and the roll inertia was 55.4 slug-ft^2. These inertias were nearly constant since the mass change during the test was small compared with the mass of the dynamic model.

Control system.- The control system to be considered herein is pictorially shown in figure 4. The thrust of four end-burning solid-propellant rocket motors provides the control forces. The control rockets are bearing mounted in a minimum-volume configuration so that rotation of two motors produces pitch control moments, rotation of the remaining two motors produces yaw control moments, and differential deflection of all four control rockets produces roll control moments. Figure 5 schematically shows the control rockets deflected to correct a positive yaw error (top view) and a positive pitch error (side view). The control-rocket deflections were limited by design to $\pm 60^\circ$. The torque to produce a control-rocket deflection is provided by a direct-current electrical drive motor. The control system has four drive motors, one geared to each control rocket. Also geared to each control rocket is a three-deck potentiometer. One deck provides control-rocket position feedback for stability, and the remaining two are used as data sensors to provide information concerning the control-rocket positions.

Guidance system.- A position and rate monitoring proportional-guidance system is employed in the experimental analysis of the control system previously discussed. The guidance system uses two two-degree-of-freedom gyros which provide inertial attitude information in roll, pitch, and yaw relative to a reference axis system defined by the spin vectors of the gyros. The guidance system also employs three rate gyros which are fixed in the spacecraft such that they measure body rates. The outputs of each gyro and the control-rocket position feedbacks are weighted and appropriately summed to provide error signals to the control system. (See fig. 3.) The numerical values and procedure for the weighting and summing are described in reference 2.

Telemetry system.- The purpose of the telemetry system was to monitor the desired performance parameters and telemeter these data to a receiving station. The system was typical of units employed in sounding-rocket flight-test research. The rate and attitude information was obtained from gyros contained in the guidance system.

The results which were obtained by the telemetry system are

(1) Roll, pitch, and yaw body rates from rate gyros

(2) Roll, pitch, and yaw attitude error angles from attitude gyros

(3) Rotational position of each control rocket

(4) Chamber pressure of control rockets

Test Apparatus

Test stand.- The test stand used in the experimental study is shown pictorially in figure 1 and schematically in figure 2. It provided a fixed rigid pivot about which the dynamic model was free to rotate. A ball and socket into which hydraulic fluid was forced under pressure constituted the pivot point. Since the hydraulic-fluid viscosity was the only source of resistance, the pivot-point friction was negligible. The point of rotational freedom was held fixed by structure securely mated with a concrete base.

Camera.- Surrounding the test stand was a structure which provided support for the photographic apparatus. (See fig. 1.) A 16-mm camera which operated at a rate of 64 frames per second was mounted above the dynamic model and viewed the model from above looking down. Also supported by the structure was a graduated framework mounted between the camera and the nose of the dynamic model.

Disturbance rockets.- Solid-fuel rocket motors with an average thrust level of 31 pounds each and a thrust duration of about 10 seconds were mounted on the dynamic model to produce known disturbances. Two disturbance rockets were located near the nose at station 36.5 inches, and two were mounted on the lower portion of the ballast at station 163 inches. The upper rockets were alined 90° apart, and the lower rockets were alined 180° apart with a distance of 10 inches between the center lines.

Restraining explosive bolts.- The dynamic model was restrained in a vertical position at the initiation of the experimental testing by two explosive bolts. These bolts were attached between the base of the dynamic model and the concrete pad located beneath the test stand. The dynamic model was free to rotate after pyrotechnic severing of the two restraining bolts.

TEST DESCRIPTION

The sequence of events for the experimental test is shown in the following table:

	Time, sec
Precess attitude gyro spin axis to define reference axis system	-4.4
Zero time for the programer used in the test	0
Control-rocket ignition	76.5
Dynamic-model release	78.5
Initiate roll attitude and rate control as well as pitch and yaw rate control	79.3
Initiate pitch and yaw attitude control to give full three-axis control	93.5
Ignite yaw disturbance rocket	99.5
Ignite roll disturbance rockets	112.9
Ignite pitch disturbance rocket	126.5

The initial orientation of the dynamic model was vertical and it was held in this position until approximately 2 seconds after control-rocket ignition at which time it was released by pyrotechnically severing the two restraining explosive bolts. After release the model was floating free with the only stabilizing forces being produced by the research control system.

The dynamic model is controlled from 0.8 second after release to termination of the experiment. The control period is divided into two phases. The first phase is defined as roll control and is effective for the first 14.2 seconds. During this time the model is subject to roll attitude and rate control as well as pitch and yaw rate control. The second phase, which is effective from $t = 93.5$ seconds to the termination of the experiment, is a three-axis control phase. During the second phase the model is controlled in attitude and rate about the roll, pitch, and yaw axes. A detailed discussion defining the requirements for this sequencing is given in reference 2.

The control task for the attitude control system of the test was to change the orientation of the model from the initially vertical position to a predetermined orientation defined by the reference angles θ_R, ψ_R, and ϕ_R. The orientation to be achieved was established by precessing the gyro spin axes so that after precession these spin axes defined an orthogonal triad, angularly displaced from the X_E-, Y_E-, and Z_E-axis system by the angles θ_R, ψ_R, and ϕ_R. (See fig. 6.) The gyro precession event occurred at $t = -4.4$ seconds. (See table.) The numerical values for the reference angles for the test were

$\theta_R = -9.5^\circ$ (pitch down)

$\psi_R = 4.7^\circ$ (yaw right)

$\phi_R = -2.5^\circ$ (roll counterclockwise)

Upon achievement of the desired inertial reference angles, the responsibility of the attitude control system was to maintain this orientation subject to disturbances.

The disturbances consisted of intentional moments acting independently about each rotational axis. Disturbance rockets were located on the dynamic model so that one produced a pitch-up disturbance, one produced a yaw-left disturbance, and the two remaining rockets produced a couple that gave a clockwise roll disturbance. The location as well as the thrust level of the rockets was such that pitch and yaw moments of about 247 foot-pounds and a roll moment of about 26 foot-pounds were realized. The magnitude of the disturbance moments was consistent with the 3σ critical disturbance characteristics of the space-vehicle upper-stage rocket motor during flight operation. The disturbances were introduced on a planar basis with the yaw disturbance first, followed by the roll disturbance, and then the pitch disturbance.

ANALYSIS AND RESULTS

General

The results of the dynamic-test-stand investigation were generated from photographic data and telemetry data. The photographic-data reduction procedure is somewhat involved and a complete description follows. The telemetry-data reduction was accomplished in a more conventional manner. The results obtained from each data source will be given in this section.

Camera Results

A camera was mounted on a structure erected around the test stand so that it viewed the model from above. Placed between the camera and the model was a fixed dimensionally graduated framework. This framework represented the Y_E,Z_E plane of the X_E-, Y_E-, and Z_E-axis system. The origin of the earth-fixed axis system lies on a fixed vertical which passes through the point of rotation of the dynamic model (bearing point). (See fig. 12.)

The nose section of the spacecraft had two black lines painted on it which crossed at a point on the nose that corresponded to a point along the longitudinal axis of the dynamic model. The two painted lines were in mutually perpendicular planes, and a black ball was fastened to the nose of the spacecraft at the point of intersection of the two lines. Figure 7 shows a typical photograph taken by the camera.

The purpose of the camera was to monitor the motion of the position-indicating ball so that data could be measured which would define the roll, pitch, and yaw Euler angles relative to the earth-fixed axis system. (See fig. 6.) The photographic data needed to define the pitch and yaw Euler angles are the coordinates of the ball in the Y_E,Z_E plane. The rotational orientation of the black stripes in a plane perpendicular to the line of sight of the camera is necessary to determine the roll Euler angle. The equations required to determine the Euler angles θ, ψ, and ϕ from the photographic data are derived and presented in appendix A as equations (A18), (A19), and (A20).

The photographic data were also employed in the determination of attitude error angles. (See fig. 6.) These angles define the orientation of the dynamic model relative to the reference axis system. The reference axis system is known relative to the earth-fixed axis system by the angles θ_R, ψ_R, and ϕ_R, and the orientation of the dynamic model is defined relative to the earth-fixed axis system by the photographically determined Euler angles. Therefore, the attitude error angles can be determined with use of the calculated Euler angles and defined reference angles. Equations for the attitude error angles θ_ϵ, ψ_ϵ, and ϕ_ϵ are derived and presented as equations (B7), (B8), and (B9) in appendix B.

The results that were obtained from the photographic data are given in figure 8. These results were obtained by processing data at 0.125-second intervals, which corresponds to using every eighth frame obtained by the camera. Roll results are presented only during roll control because of inaccuracies in the roll data after three-axis control when the nose of the model is rotated away from the line of sight of the camera. Figure 8(a) shows the Euler angles that were determined by using equations (A18), (A19), and (A20). This plot gives an attitude time history of the dynamic model during the experimental test. The zero value for each parameter refers to the initial orientation, and the dashed lines represent the inertial reference angles which define the attitude to be achieved.

The closed-loop system comprised of the research control system, guidance system, and model exhibits type-0 servosystem steady-state characteristics (ref. 3); that is, in order to produce a steady control deflection to balance a steady external moment, a steady actuating (attitude) error must be present. For this reason an attitude error is present during the time period the disturbance rockets are functioning. This error is represented by the deviations of the Euler angles from the reference values and occurs in each plane corresponding to the presence of a planned disturbance. (See fig. 8(a).)

Figure 8(b) shows the variation of the roll, pitch, and yaw attitude error angles with time. These angles were computed from camera data with the use of equations (B7), (B8), and (B9). Zero values for the gyro angles correspond to the dynamic model alined with the reference axis system. The steady-state error discussed previously is shown in figure 8(b).

Telemetry Results

Control-rocket thrust.- Pressure transducers were utilized to monitor the chamber pressure of each control rocket, and the results were telemetered to a receiving station. The chamber pressure was utilized to compute the thrust or available control force of the control rockets. The thrust was determined by using equations given in reference 4. The transducer of control rocket number 2 did not function properly; therefore, only three thrust time histories were determined and these are shown in figure 9. The dashed curve represents an average of the experimentally determined results.

Control parameters.- Figure 10 presents time histories of the attitude error angles, body rotational velocity components, and control-rocket positions that were obtained by telemetry. The attitude error angles are given in figure 10(a). The outputs of the pitch and yaw attitude gyros were grounded to zero during roll control, which was necessary since the pitch and yaw attitude information is not used for control during this period.

Figure 10(b) gives the variation with time of the body rotational velocity components p, q, and r which were sensed by rate gyros contained in the guidance system. The transients associated with release, roll capture, and three-axis capture can be seen in this figure.

Figure 10(c) shows the position variation of each control rocket with time. These data were obtained by telemetry from the position-indicating potentiometers geared to the control rockets. For each control rocket one deck of the potentiometer provided data within $\pm 10^{\circ}$ boundaries to give good position-data resolution. The other data deck measured positions between $\pm 60^{\circ}$. These two sources were combined to give the results presented in figure 10(c) where, for control rocket number 4, no data are shown beyond the $\pm 10^{\circ}$ boundaries. The steady-state deflections needed to control the intentional disturbances can also be seen in figure 10(c).

COMPARISON AND DISCUSSION OF ANALOG AND EXPERIMENTAL RESULTS

A graphical comparison between the results obtained from the experimental test and the results obtained from the analog simulation is given in figure 11 where the experimental results are a repeat of previous presentations in this report. The analog simulation makes use of the equations presented in appendix C.

Figure 11(a) shows a comparison of the Euler angles determined photographically (experimental) with those determined by the analog analysis. An examination of the photographically determined roll Euler angle shows that the model rolled positively during the time interval between release and the beginning of control. This positive roll was apparently the result of an extraneous torque, possibly produced by the separation mechanism. This motion is not shown in the analog results because the moment was not defined and was not included in the analog simulation.

Time histories of the pitch Euler angle show that the model was under the influence of a negative pitching moment, which was probably the result of winds and other external disturbances. This extraneous moment was estimated to be about -55 foot-pounds and was included in the analog simulation. The camera-determined yaw Euler angle diverges ($t \approx 122$ sec) from the defined reference value represented by the dashed line. This divergence is apparently caused by a drift of the gyro spin axis which defines the inertial reference. (In order to represent this drift in figure 8(a), the dashed line would be curved upward.) Since a constant reference was used in the analog analysis, this divergence is not noted in the analog results.

The analog and camera Euler-angle results agree extremely well except for the explainable differences which are caused primarily by detailed disturbances that are not definable in the analog representation. The primary criteria for comparison are dynamic stability and damping characteristics.

Figures 11(b), 11(c), and 11(d) give the variations of the attitude error angles with time. Since the experimental results were obtained from both telemetry and photography, a three-way comparison was possible between these results and those from the analog analysis. Because the telemetry results are unavailable during roll control, a portion of the comparison is lost. Much of the same basic discussion presented with the Euler angle results applies to the error-angle comparison, and as with the Euler angle comparison, the agreement is good. Although there are numerical differences, especially with the telemetry data, the damping characteristics obtained from all three sources are comparable.

Figure 11(e) gives a comparison of the rotational velocity components p, q, and r obtained by telemetry (experimental) and those obtained by analog simulation. Two pronounced points of disagreement are at roll capture and pitch capture. The roll capture disagreement was previously explained as a disturbance which was not included in the analog simulation. The same explanation applies to the pitch-capture disagreement as exemplified by the fact that the rate q was returning to zero when a disturbance redirected it in a negative direction. Much of the low-amplitude oscillation noted in the figure results from the control rockets deflecting indeterminately within unintentional and uncorrectable deadbands. A detailed comparison of the rotational-velocity results is not considered to be realistic; however, a survey of all transients shows good dynamic-stability agreement.

A comparison of the control-rocket position time histories is given in figures 11(f) and 11(g). The oscillatory wave which appears to be riding on the deflection traces is the result of system nonlinearities. The steady-state deflections needed to control the intentional disturbances are seen by reviewing the figures. The graphical comparison of the control-rocket deflection results shows good agreement.

CONCLUDING REMARKS

The results obtained from a dynamic-test-stand investigation of a space-vehicle upper stage employing actual electro-mechanical systems have been presented. Experimental data received from an onboard telemetry system and a unique photographic technique were presented and compared with the results obtained from an analog simulation of the dynamical system.

The Euler angles determined from photographic data showed good agreement with the analog-study results as did the attitude error angles computed from the camera data and those obtained in the analog study. A comparison between the attitude error angles obtained from these data sources and those reduced from telemetry data also showed good agreement in most areas. The body rotational velocity components obtained from telemetry and those obtained from the analog simulation showed the same general trends. The control-rocket position histories from these two data sources were in reasonable agreement. These comparisons also showed that although telemetry results were somewhat limited in accuracy, the telemeter data can be used for a comprehensive analysis of the dynamical system.

The analog simulation employed herein was also used to analyze and define system gains and sequences in a previous analysis of the space-vehicle upper stage. Since this dynamical system functioned as predicted by the analog study, it is concluded that the analog simulation is an adequate mathematical representation of the dynamical system.

Langley Research Center,
National Aeronautics and Space Administration,
Langley Station, Hampton, Va., May 12, 1965.

APPENDIX A

EQUATIONS FOR REDUCING CAMERA DATA

Equations are developed in this appendix which define the attitude of the dynamic model as a function of parameters obtained from photographic data. The data obtained by the camera technique employed in the dynamic-test-stand investigation are the coordinates of P' (see fig. 12) and a protractor-determined roll angle. The coordinates of P' do not represent the true coordinates of the position-indicating ball in the Y_E,Z_E plane due to parallax. The true coordinates are represented by the point P. The measured roll angle also does not represent the true roll angle, because the line of sight of the camera is not along the longitudinal axis of the dynamic model. Because the raw photographic data must be corrected prior to determination of the desired attitude angles, the correction equations will be presented first followed by a presentation of the attitude equations.

DATA CORRECTION EQUATIONS

The initial problem is one of defining relationships so that the coordinates of P' can be corrected to give the coordinates of P, and the protractor-measured roll angle can be corrected to give the true roll angle.

The two right triangles shown in figure 12 with the Y_E-axis as one leg, apexes at point O, and hypotenuses $\overline{OP'}$ and $\overline{OP}$ are similar; therefore,

$$\frac{y'_E}{\overline{OP'}} = \frac{y_E}{\overline{OP}} \tag{A1}$$

and

$$\frac{z'_E}{\overline{OP'}} = \frac{z_E}{\overline{OP}} \tag{A2}$$

These equations can be modified to give the following:

$$y_E = \frac{y'_E}{\sqrt{\left(y'_E\right)^2 + \left(z'_E\right)^2}}\,\overline{OP} \tag{A3}$$

and

$$z_E = \frac{z'_E}{\sqrt{\left(y'_E\right)^2 + \left(z'_E\right)^2}} \overline{OP} \tag{A4}$$

In order to solve equations (A3) and (A4) it is necessary to define $\overline{OP}$. From figure 12 it can be seen that

$$\overline{OP} = r_m \sin \beta \tag{A5}$$

where r_m is known and a relationship for $\sin \beta$ must be determined.

Equation (A6) is the law of sines for the triangle containing the angles α, β, and ω.

$$\frac{r_m}{\sin \alpha} = \frac{\overline{CB}}{\sin \beta} = \frac{h + e + r_m}{\sin \omega} \tag{A6}$$

From equation (A6)

$$\sin \beta = \frac{\overline{CB}}{r_m} \sin \alpha \tag{A7}$$

and $\overline{CB}$ can be defined as

$$\overline{CB} = (h + e + r_m)\cos \alpha + r_m \cos \omega \tag{A8}$$

Also, from equation (A6)

$$\sin \omega = \frac{h + e + r_m}{r_m} \sin \alpha \tag{A9}$$

and from figure 12 $\sin \alpha$ may be expressed as follows:

$$\sin \alpha = \frac{\overline{OP'}}{\sqrt{h^2 + \overline{OP'}^2}} \tag{A10}$$

Use of equations (A9) and (A10) in substituting for the cosine functions of α and ω in equation (A8) gives

$$\overline{CB} = (h + e + r_m)\sqrt{\frac{\left(h^2 + \overline{OP'}^2 - \overline{OP'}^2\right)}{h^2 + \overline{OP'}^2}} - \sqrt{\frac{r_m^2\left(h^2 + \overline{OP'}^2\right) - (h + e + r_m)^2\overline{OP'}^2}{h^2 + \overline{OP'}^2}} \tag{A11}$$

The negative sign of the second radical of equation (A11) is necessary since ω is greater than 90° for all applications in this report. Combining equations (A7), (A10), and (A11) gives

$$\sin \beta = \frac{\overline{OP'}}{r_m\left(h^2 + \overline{OP'}^2\right)}\left[h(h + e + r_m) - \sqrt{r_m^2\left(h^2 + \overline{OP'}^2\right) - \overline{OP'}^2(h + e + r_m)^2}\right] \tag{A12}$$

Equations (A3), (A4), (A5), and (A12) can now be combined to give

$$y_E = y'_E\left\{\frac{h(h + e + r_m) - \sqrt{r_m^2\left[h^2 + \left(y'_E\right)^2 + \left(z'_E\right)^2\right] - \left[\left(y'_E\right)^2 + \left(z'_E\right)^2\right](h + e + r_m)^2}}{h^2 + \left(y'_E\right)^2 + \left(z'_E\right)^2}\right\} \tag{A13}$$

and

$$z_E = z'_E\left\{\frac{h(h + e + r_m) - \sqrt{r_m^2\left[h^2 + \left(y'_E\right)^2 + \left(z'_E\right)^2\right] - \left[\left(y'_E\right)^2 + \left(z'_E\right)^2\right](h + e + r_m)^2}}{h^2 + \left(y'_E\right)^2 + \left(z'_E\right)^2}\right\} \tag{A14}$$

Equations (A13) and (A14) define the true coordinates y_E and z_E of the position-indicating ball in the Y_E, Z_E plane.

The protractor-measured roll angle ϕ' is in a plane perpendicular to the line of sight of the camera. The true roll angle ϕ is in a plane perpendicular to the longitudinal axis of the dynamic model. Therefore, the measured roll angle must be projected into the desired plane. The following equation defines this projection:

$$\sin \phi' = \cos \eta \sin \phi \tag{A15}$$

The value of $\cos \eta$ is the unknown in equation (A15) which must be defined. Since η and ω are supplementary angles, η may be expressed in terms of ω as

$$\eta = 180 - \omega \tag{A16}$$

and by combining equations (A16) and (A9)

$$\cos \eta = \sqrt{\frac{r_m^2\left(h^2 + \overline{OP'}^2\right) - \left(h + e + r_m\right)^2\overline{OP'}^2}{r_m^2\left(h^2 + \overline{OP'}^2\right)}} \tag{A17}$$

Equations (A15) and (A17) can be used to define the true roll angle ϕ as follows:

$$\sin \phi = \sin \phi' \sqrt{\frac{r_m^2\left[h^2 + \left(y'_E\right)^2 + \left(z'_E\right)^2\right]}{r_m^2\left[h^2 + \left(y'_E\right)^2 + \left(z'_E\right)^2\right] - \left(h + e + r_m\right)^2\left[\left(y'_E\right)^2 + \left(z'_E\right)^2\right]}} \tag{A18}$$

Equations (A13), (A14), and (A18) yield the results needed to define the attitude of the dynamic model as a function of the raw photographic data.

ANGULAR ATTITUDE EQUATIONS

Euler angles θ, ψ, and ϕ define the attitude of the dynamic model in the X_E-, Y_E-, and Z_E-axis system. The sine of the roll Euler angle was given by equation (A18), and the pitch and yaw Euler angles are defined by the following equations:

$$\theta = \sin^{-1}\left(\frac{-z_E}{r_m}\right) \tag{A19}$$

$$\psi = \sin^{-1}\left(\frac{y_E}{\sqrt{r_m^2 - z_E^2}}\right) \tag{A20}$$

APPENDIX B

EQUATIONS USED IN DETERMINING ATTITUDE ERROR ANGLE

Equations were derived in reference 2 which defined the attitude error angles in terms of Euler angles and a pitch reference angle. A similar derivation is presented in this appendix in order to define the attitude error angles in terms of Euler angles and roll, pitch, and yaw reference angles. The derivation consists of a series of orthogonal transformations between axis systems. Figure 6 serves as a useful tool in reviewing the following derivation.

The transformation between the earth-fixed axis system $(X_E,\ Y_E,$ and $Z_E)$ and the body axis system is

$$\begin{bmatrix} X \\ Y \\ Z \end{bmatrix} = \begin{bmatrix} 1 & 0 & 0 \\ 0 & \cos\phi & \sin\phi \\ 0 & -\sin\phi & \cos\phi \end{bmatrix} \begin{bmatrix} \cos\theta & 0 & -\sin\theta \\ 0 & 1 & 0 \\ \sin\theta & 0 & \cos\theta \end{bmatrix} \begin{bmatrix} \cos\psi & \sin\psi & 0 \\ -\sin\psi & \cos\psi & 0 \\ 0 & 0 & 1 \end{bmatrix} \begin{bmatrix} X_E \\ Y_E \\ Z_E \end{bmatrix} \tag{B1}$$

which, when simplified, becomes

$$\begin{bmatrix} X \\ Y \\ Z \end{bmatrix} = \begin{bmatrix} \cos\theta\cos\psi & \cos\theta\sin\psi & -\sin\theta \\ \sin\phi\sin\theta\cos\psi - \cos\phi\sin\psi & \sin\phi\sin\theta\sin\psi + \cos\phi\cos\psi & \sin\phi\cos\theta \\ \cos\phi\sin\theta\cos\psi + \sin\phi\sin\psi & \cos\phi\sin\theta\sin\psi - \sin\phi\cos\psi & \cos\phi\cos\theta \end{bmatrix} \begin{bmatrix} X_E \\ Y_E \\ Z_E \end{bmatrix} \tag{B2}$$

The transformation between the earth-fixed axis system and the reference axis system is

$$\begin{bmatrix} X_R \\ Y_R \\ Z_R \end{bmatrix} = \begin{bmatrix} \cos\theta_R\cos\psi_R & \cos\theta_R\sin\psi_R & -\sin\theta_R \\ \sin\phi_R\sin\theta_R\cos\psi_R - \cos\phi_R\sin\psi_R & \sin\phi_R\sin\theta_R\sin\psi_R + \cos\phi_R\cos\psi_R & \sin\theta_R\cos\theta_R \\ \cos\phi_R\sin\theta_R\cos\psi_R + \sin\phi_R\sin\psi_R & \cos\phi_R\sin\theta_R\sin\psi_R - \sin\phi_R\cos\psi_R & \cos\phi_R\cos\theta_R \end{bmatrix} \begin{bmatrix} X_E \\ Y_E \\ Z_E \end{bmatrix} \tag{B3}$$

APPENDIX B

By transposing equation (B3) and substituting the results into equation (B2), the following equation is obtained:

$$
\begin{bmatrix} X \\ Y \\ Z \end{bmatrix} = \begin{bmatrix}
\cos\theta\cos\psi\cos\theta_R\cos\psi_R + \cos\theta\sin\psi\cos\theta_R\sin\psi_R + \sin\theta\sin\theta_R & \cos\theta\cos\psi\sin\phi_R\sin\theta_R\cos\psi_R - \cos\theta\cos\psi\cos\phi_R\sin\psi_R + \cos\theta\sin\psi\sin\phi_R\sin\theta_R\sin\psi_R + \cos\theta\sin\psi\cos\phi_R\cos\psi_R - \sin\theta\sin\phi_R\cos\theta_R & \cos\theta\cos\psi\cos\phi_R\sin\theta_R\cos\psi_R + \cos\theta\cos\psi\sin\phi_R\sin\psi_R + \cos\theta\sin\psi\cos\phi_R\sin\theta_R\sin\psi_R - \cos\theta\sin\psi\sin\phi_R\cos\psi_R - \sin\theta\cos\phi_R\cos\theta_R \\
\sin\phi\sin\theta\cos\psi\cos\theta_R\cos\psi_R - \cos\phi\sin\psi\cos\theta_R\cos\psi_R + \sin\phi\sin\theta\sin\psi\cos\theta_R\sin\psi_R + \cos\phi\cos\psi\cos\theta_R\sin\psi_R - \sin\phi\cos\theta\sin\theta_R & \sin\phi\sin\theta\cos\psi\sin\phi_R\sin\theta_R\cos\psi_R - \sin\phi\sin\theta\cos\psi\cos\phi_R\sin\psi_R - \cos\phi\sin\psi\sin\phi_R\sin\theta_R\cos\psi_R + \cos\phi\sin\psi\cos\phi_R\sin\psi_R + \sin\phi\sin\theta\sin\psi\sin\phi_R\sin\theta_R\sin\psi_R + \sin\phi\sin\theta\sin\psi\cos\phi_R\cos\psi_R + \cos\phi\cos\psi\sin\phi_R\sin\theta_R\sin\psi_R + \cos\phi\cos\psi\cos\phi_R\cos\psi_R + \sin\phi\cos\theta\sin\phi_R\cos\theta_R & \sin\phi\sin\theta\cos\psi\cos\phi_R\sin\theta_R\cos\psi_R + \sin\phi\sin\theta\cos\psi\sin\phi_R\sin\psi_R - \cos\phi\sin\psi\cos\phi_R\sin\theta_R\cos\psi_R - \cos\phi\sin\psi\sin\phi_R\sin\psi_R + \sin\phi\sin\theta\sin\psi\cos\phi_R\sin\theta_R\sin\psi_R - \sin\phi\sin\theta\sin\psi\sin\phi_R\cos\psi_R + \cos\phi\cos\psi\cos\phi_R\sin\theta_R\sin\psi_R - \cos\phi\cos\psi\sin\phi_R\cos\psi_R + \sin\phi\cos\theta\cos\phi_R\cos\theta_R \\
\cos\phi\sin\theta\cos\psi\cos\theta_R\cos\psi_R + \sin\phi\sin\psi\cos\theta_R\cos\psi_R + \cos\phi\sin\theta\sin\psi\cos\theta_R\sin\psi_R - \sin\phi\cos\psi\cos\theta_R\sin\psi_R - \cos\phi\cos\theta\sin\theta_R & \cos\phi\sin\theta\cos\psi\sin\phi_R\sin\theta_R\cos\psi_R - \cos\phi\sin\theta\cos\psi\cos\phi_R\sin\psi_R + \sin\phi\sin\psi\sin\phi_R\sin\theta_R\cos\psi_R - \sin\phi\sin\psi\cos\phi_R\sin\psi_R + \cos\phi\sin\theta\sin\psi\sin\phi_R\sin\theta_R\sin\psi_R + \cos\phi\sin\theta\sin\psi\cos\phi_R\cos\psi_R - \sin\phi\cos\psi\sin\phi_R\sin\theta_R\sin\psi_R - \sin\phi\cos\psi\cos\phi_R\cos\psi_R + \cos\phi\cos\theta\sin\phi_R\cos\theta_R & \cos\phi\sin\theta\cos\psi\cos\phi_R\sin\theta_R\cos\psi_R + \cos\phi\sin\theta\cos\psi\sin\phi_R\sin\psi_R + \sin\phi\sin\psi\cos\phi_R\sin\theta_R\cos\psi_R + \sin\phi\sin\psi\sin\phi_R\sin\psi_R + \cos\phi\sin\theta\sin\psi\cos\phi_R\sin\theta_R\sin\psi_R - \cos\phi\sin\theta\sin\psi\sin\phi_R\cos\psi_R - \sin\phi\cos\psi\cos\phi_R\sin\theta_R\sin\psi_R + \sin\phi\cos\psi\sin\phi_R\cos\psi_R + \cos\phi\cos\theta\cos\phi_R\cos\theta_R
\end{bmatrix} \begin{bmatrix} X_R \\ Y_R \\ Z_R \end{bmatrix} \tag{B4}
$$

Equation (B4) represents a transformation between the body axes and the reference axes. An additional transformation between the body axes and the reference axes is as follows:

$$
\begin{bmatrix} X \\ Y \\ Z \end{bmatrix} = \begin{bmatrix}
\cos\theta_\epsilon\cos\psi^*_\epsilon & \cos\theta_\epsilon\sin\psi^*_\epsilon & -\sin\theta_\epsilon \\
\sin\phi_\epsilon\sin\theta_\epsilon\cos\psi^*_\epsilon - \cos\phi_\epsilon\sin\psi^*_\epsilon & \sin\phi_\epsilon\sin\theta_\epsilon\sin\psi^*_\epsilon + \cos\phi_\epsilon\cos\psi^*_\epsilon & \sin\phi_\epsilon\cos\theta_\epsilon \\
\cos\phi_\epsilon\sin\theta_\epsilon\cos\psi^*_\epsilon + \sin\phi_\epsilon\sin\psi^*_\epsilon & \cos\phi_\epsilon\sin\theta_\epsilon\sin\psi^*_\epsilon - \sin\phi_\epsilon\cos\psi^*_\epsilon & \cos\phi_\epsilon\cos\theta_\epsilon
\end{bmatrix} \begin{bmatrix} X_R \\ Y_R \\ Z_R \end{bmatrix} \tag{B5}
$$

Since the attitude error angle is measured in the plane of the dynamic model and the yaw angle ψ^*_ϵ noted in the transformation is the projection of the attitude error angle in the reference X_R, Y_R plane, the following expression is necessary to define the yaw attitude error angle:

$$\sin\psi_\epsilon = \sin\psi^*_\epsilon\cos\theta_\epsilon \tag{B6}$$

APPENDIX B

By equating the equal elements of (B4) and (B5), the following attitude-error-angle equations are obtained:

$$\begin{aligned}\sin\theta_\epsilon = &-\cos\theta\cos\psi\cos\phi_R\sin\theta_R\cos\psi_R\\ &-\cos\theta\cos\psi\sin\phi_R\sin\psi_R\\ &-\cos\theta\sin\psi\cos\phi_R\sin\theta_R\sin\psi_R\\ &+\cos\theta\sin\psi\sin\phi_R\cos\psi_R\\ &+\sin\theta\cos\phi_R\cos\theta_R\end{aligned} \tag{B7}$$

$$\begin{aligned}\sin\psi_\epsilon = &\cos\theta\cos\psi\sin\phi_R\sin\theta_R\cos\psi_R\\ &-\cos\theta\cos\psi\cos\phi_R\sin\psi_R\\ &+\cos\theta\sin\psi\sin\phi_R\sin\theta_R\sin\psi_R\\ &+\cos\theta\sin\psi\cos\phi_R\cos\psi_R\\ &-\sin\theta\sin\phi_R\cos\theta_R\end{aligned} \tag{B8}$$

$$\begin{aligned}\sin\phi_\epsilon\cos\theta_\epsilon = &\sin\phi\sin\theta\cos\psi\cos\phi_R\sin\theta_R\cos\psi_R\\ &+\sin\phi\sin\theta\cos\psi\sin\phi_R\sin\psi_R\\ &-\cos\phi\sin\psi\cos\phi_R\sin\theta_R\cos\psi_R\\ &-\cos\phi\sin\psi\sin\phi_R\sin\psi_R\\ &+\sin\phi\sin\theta\sin\psi\cos\phi_R\sin\theta_R\sin\psi_R\\ &-\sin\phi\sin\theta\sin\psi\sin\phi_R\cos\psi_R\\ &+\cos\phi\cos\psi\cos\phi_R\sin\theta_R\sin\psi_R\\ &-\cos\phi\cos\psi\sin\phi_R\cos\psi_R\\ &+\sin\phi\cos\theta\cos\phi_R\cos\theta_R\end{aligned} \tag{B9}$$

APPENDIX C

EQUATIONS USED IN ANALOG COMPUTER ANALYSIS

The mathematical descriptions of the dynamical systems used to generate the results presented in this report are the same as those given in reference 2 except for the vehicle and trajectory simulation. The representation for the vehicle and trajectory simulation of this investigation is given by the following equations and differs from that of reference 2 because no translation occurred during the dynamic test:

$$\dot{p}I_X = -F\left(\sin \delta_1 - \sin \delta_3 - \sin \delta_2 + \sin \delta_4\right)x_p + M_X \tag{C1}$$

$$\dot{q}I_Y + rpI_X - rpI_Z = -F\left(\sin \delta_2 + \sin \delta_4\right)\left(x_{cr} - x_q\right) + M_Y \tag{C2}$$

$$\dot{r}I_Z + pqI_Y - pqI_X = -F\left(\sin \delta_1 + \sin \delta_3\right)\left(x_{cr} - x_r\right) + M_Z \tag{C3}$$

$$\dot{\psi} = \frac{q \sin \phi + r \cos \phi}{\cos \theta} \tag{C4}$$

$$\dot{\phi} = p + \dot{\psi} \sin \theta \tag{C5}$$

$$\dot{\theta} = q \cos \phi - r \sin \phi \tag{C6}$$

$$\psi = \int_t \dot{\psi}\, dt + \psi_o \tag{C7}$$

$$\phi = \int_t \dot{\phi}\, dt + \phi_o \tag{C8}$$

$$\theta = \int_t \dot{\theta}\, dt + \theta_o \tag{C9}$$

REFERENCES

1. Fall, R. C.; Koch, Robert L.; and DeBord, C. J.: Development of the Rocket Velocity and Attitude Control System. Eng. Dept. Rept. No. 2137 (Contract No. NAS 5-483), Allison Div., Gen. Motors Corp., May 29, 1961.

2. Young, A. Thomas; and Harris, Jack E.: An Analog Study of a Rotating-Solid-Rocket Control System and Its Application to Attitude Control of a Space-Vehicle Upper Stage. NASA TN D-2366, 1964.

3. Nixon, Floyd E.: Principles of Automatic Controls. Prentice-Hall, Inc., c.1953.

4. Barrère, Marcel; Jaumotte, André; De Veubeke, Baudouin Fraeijs; and Vandenkerckhove, Jean: Rocket Propulsion. Elsevier Pub. Co., 1960.

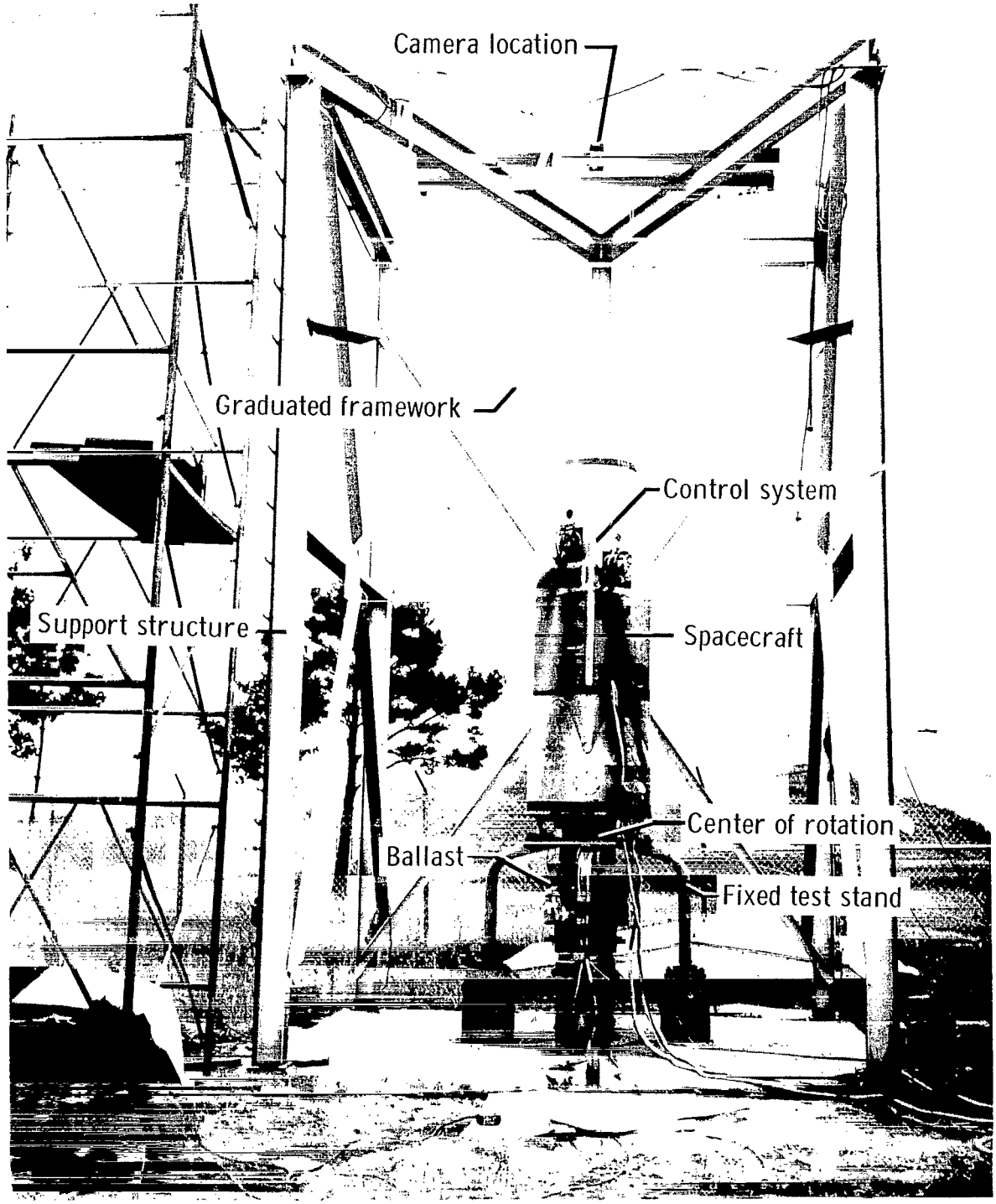

Figure 1.- Photograph of test setup. L-64-5760.1

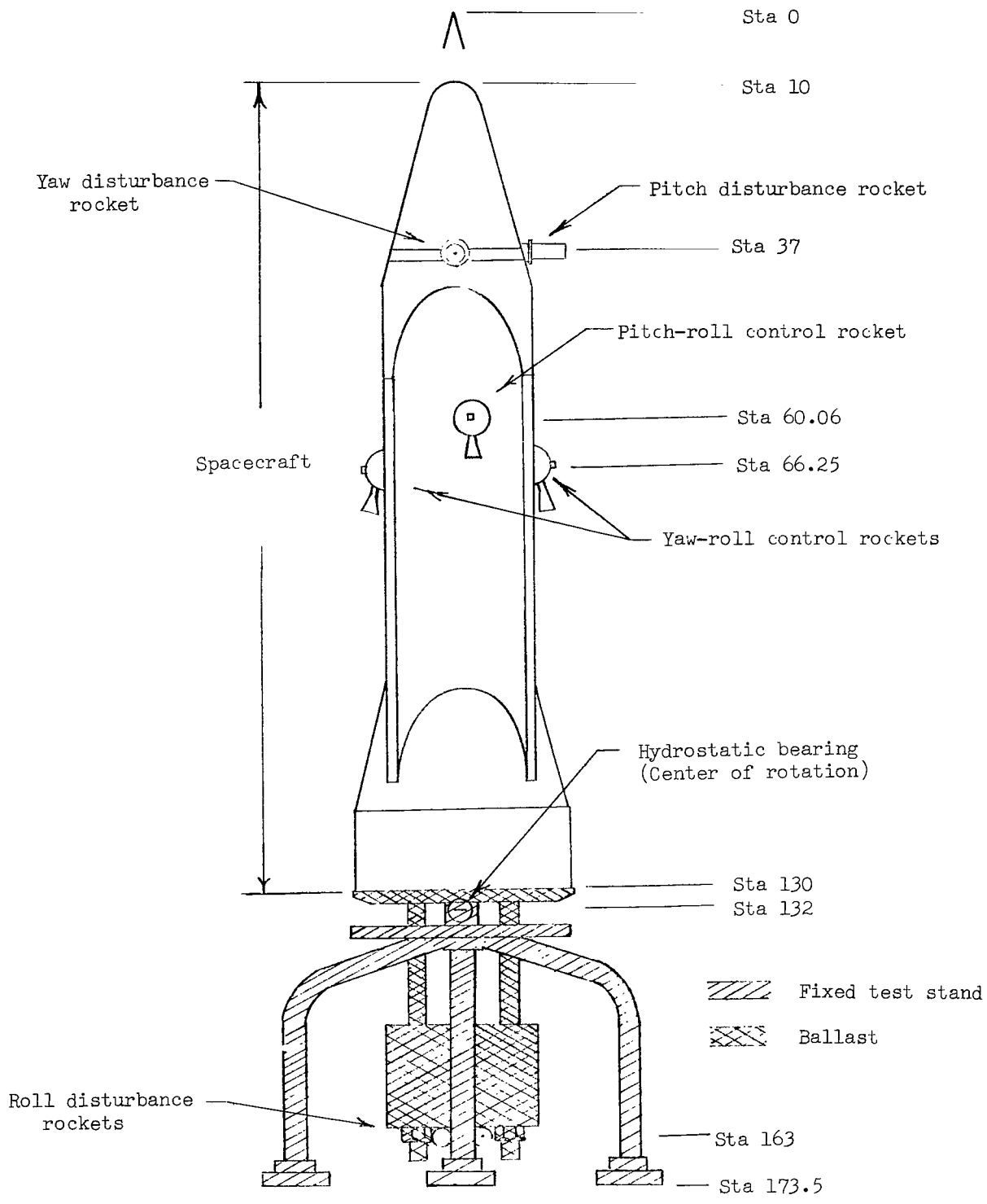

Figure 2.- General arrangement of dynamic model and test stand. Stations are in inches.

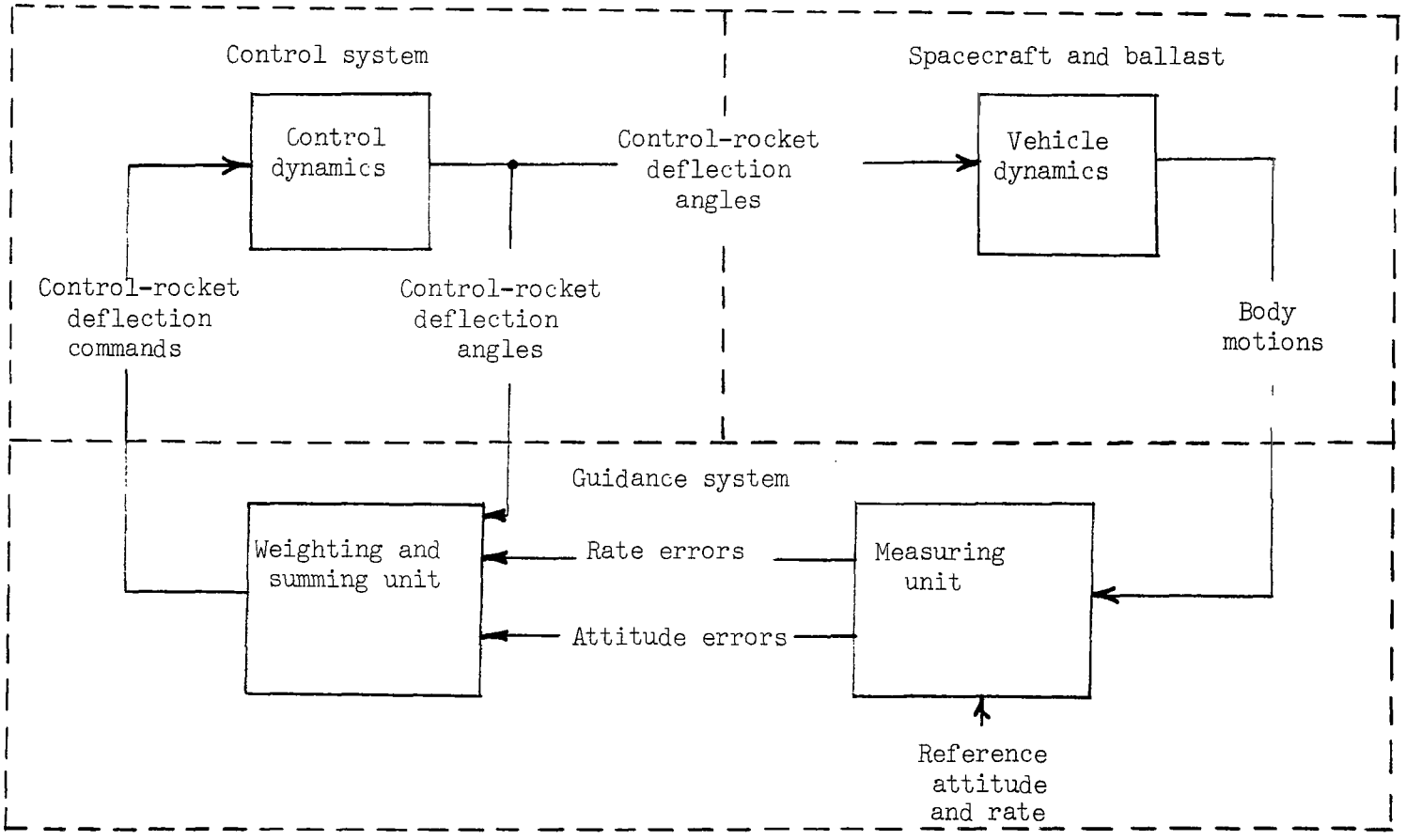

Figure 3.- Block diagram of major elements of dynamic model.

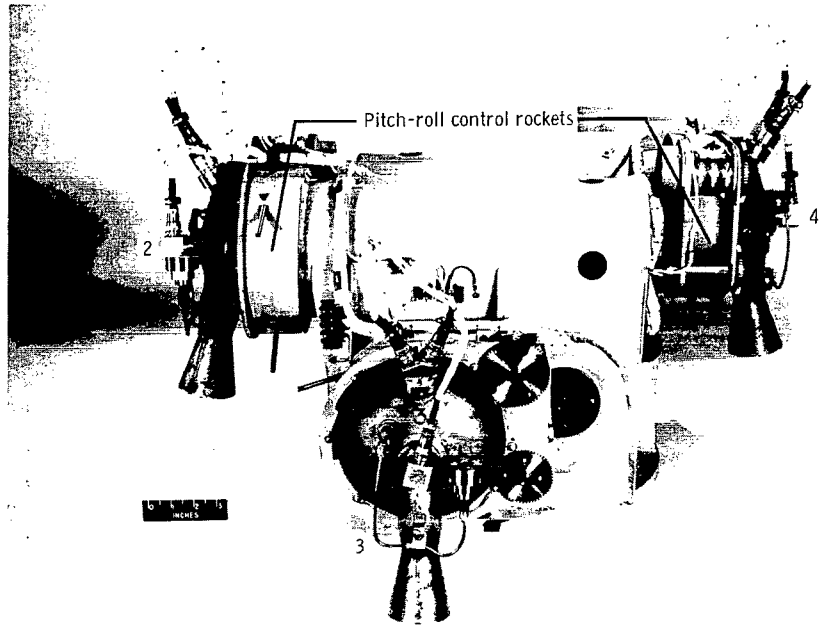

L-63-8714.1

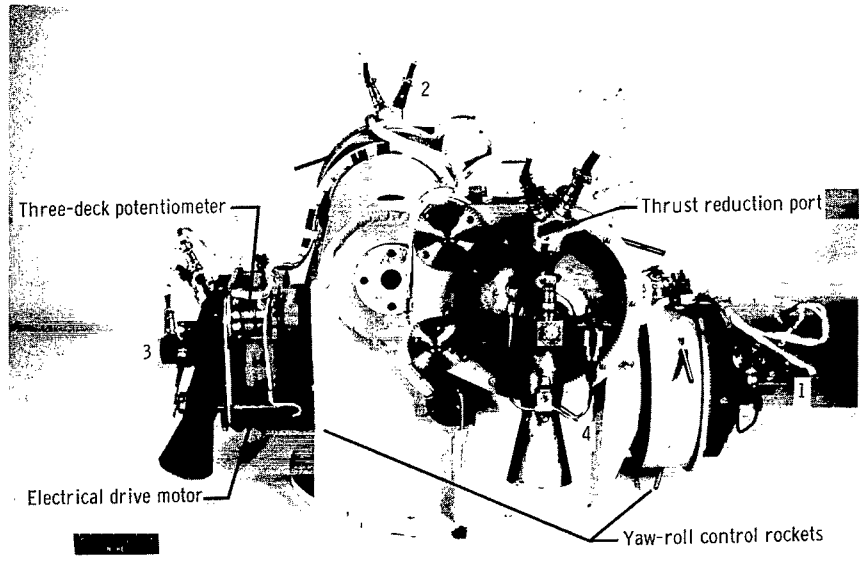

Figure 4.- Photograph of control system. Numbers designate control rockets. L-63-8715.1

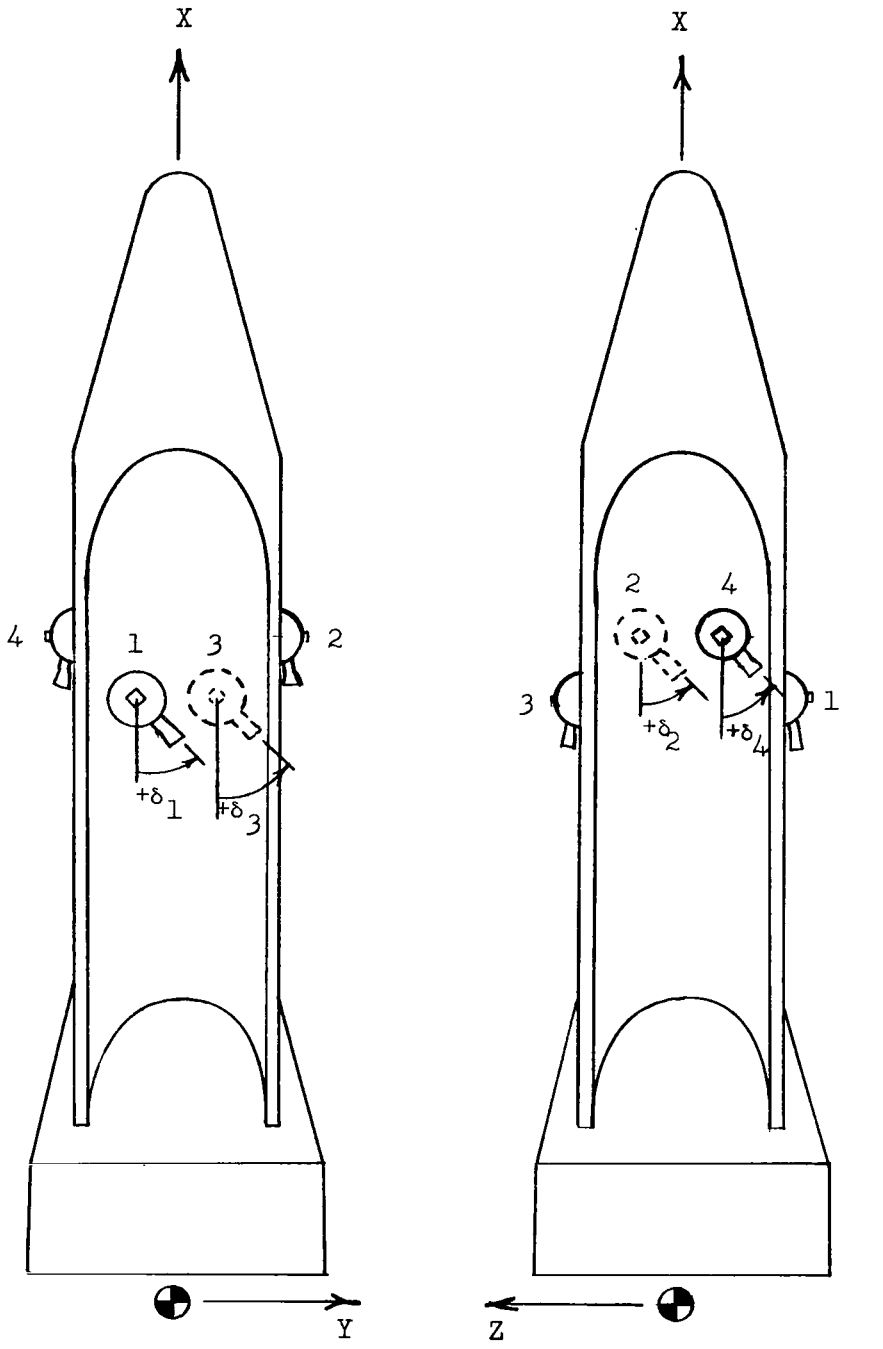

Figure 5.- Sketch showing control rocket deflection convention.

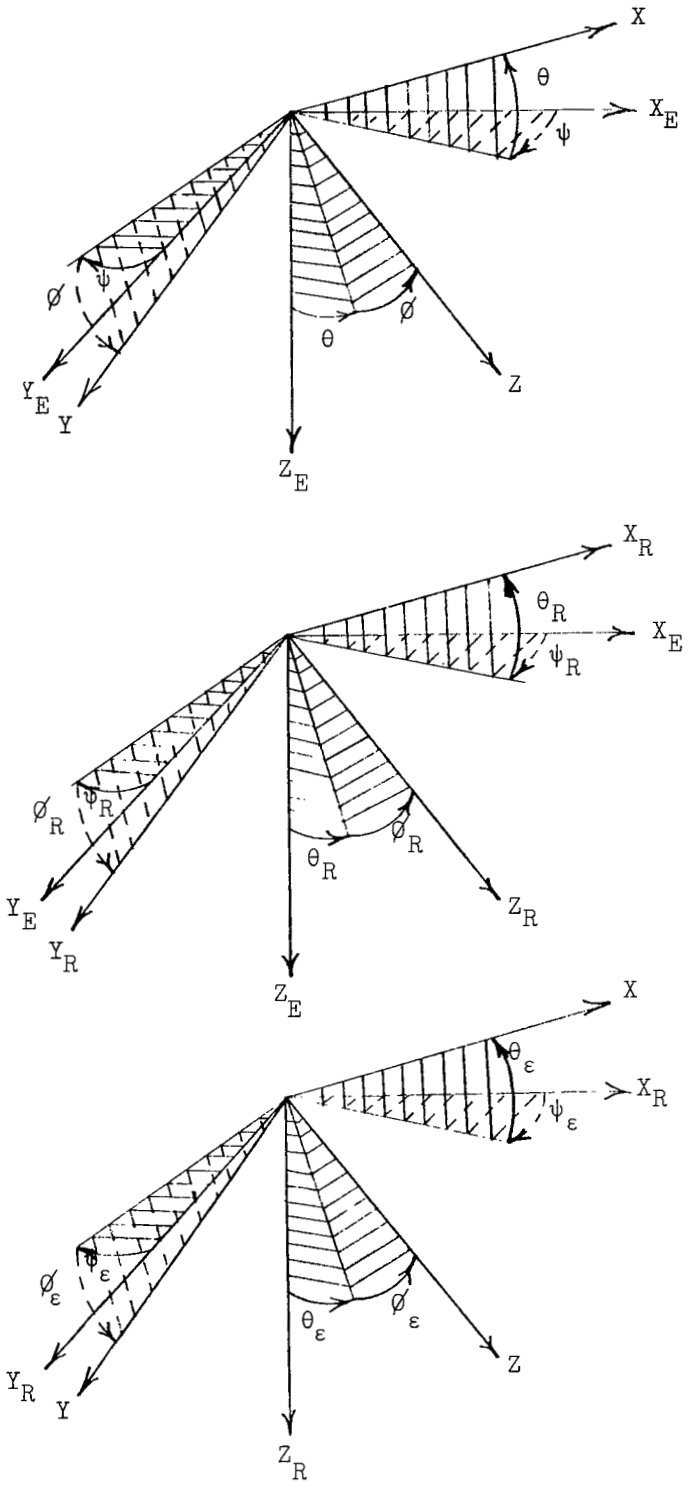

Figure 6.- Schematic relationship between axis systems. All angles shown are positive.

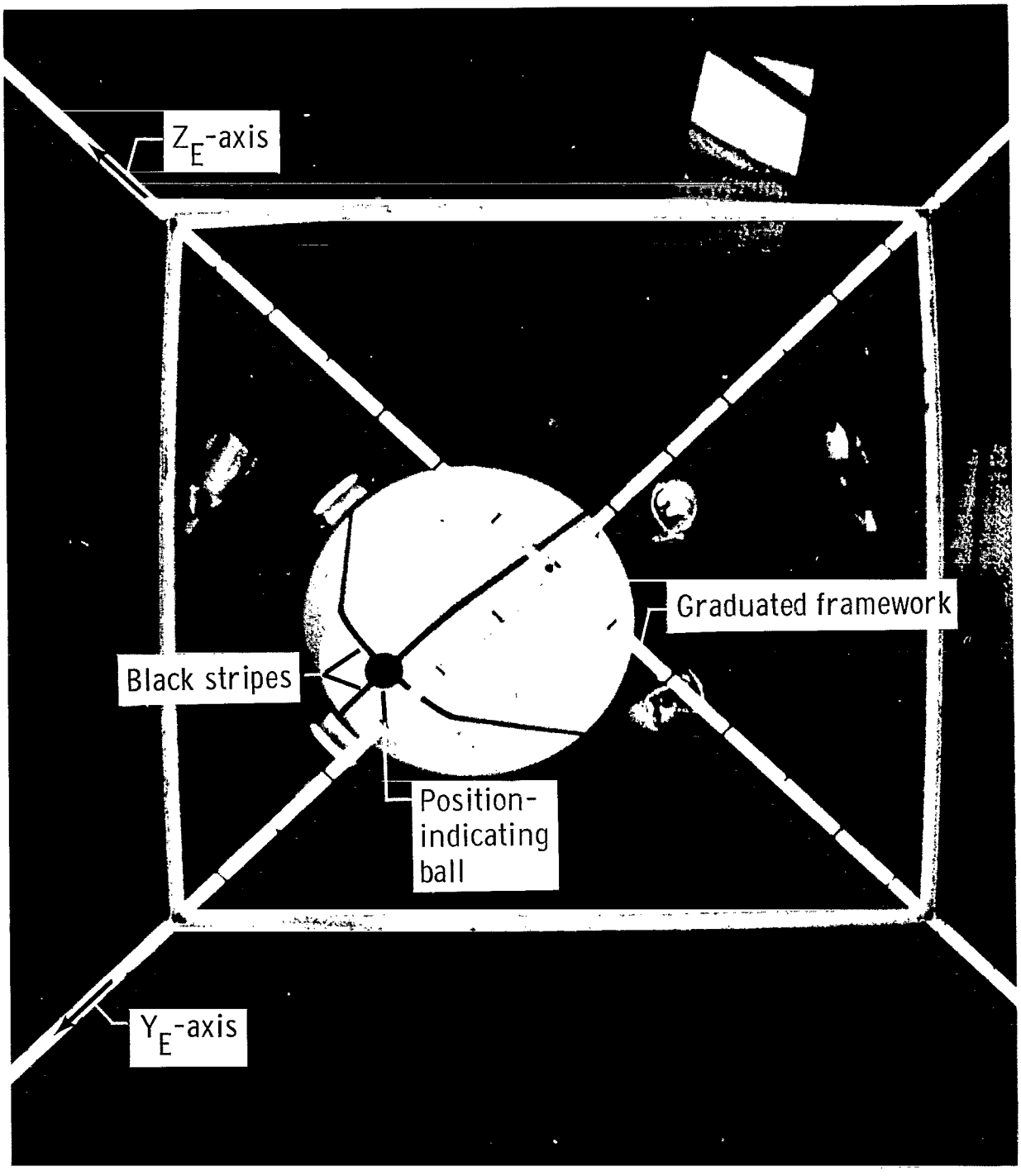

Figure 7.- Typical view from top camera. Each graduation equal to 3 inches. L-65-137

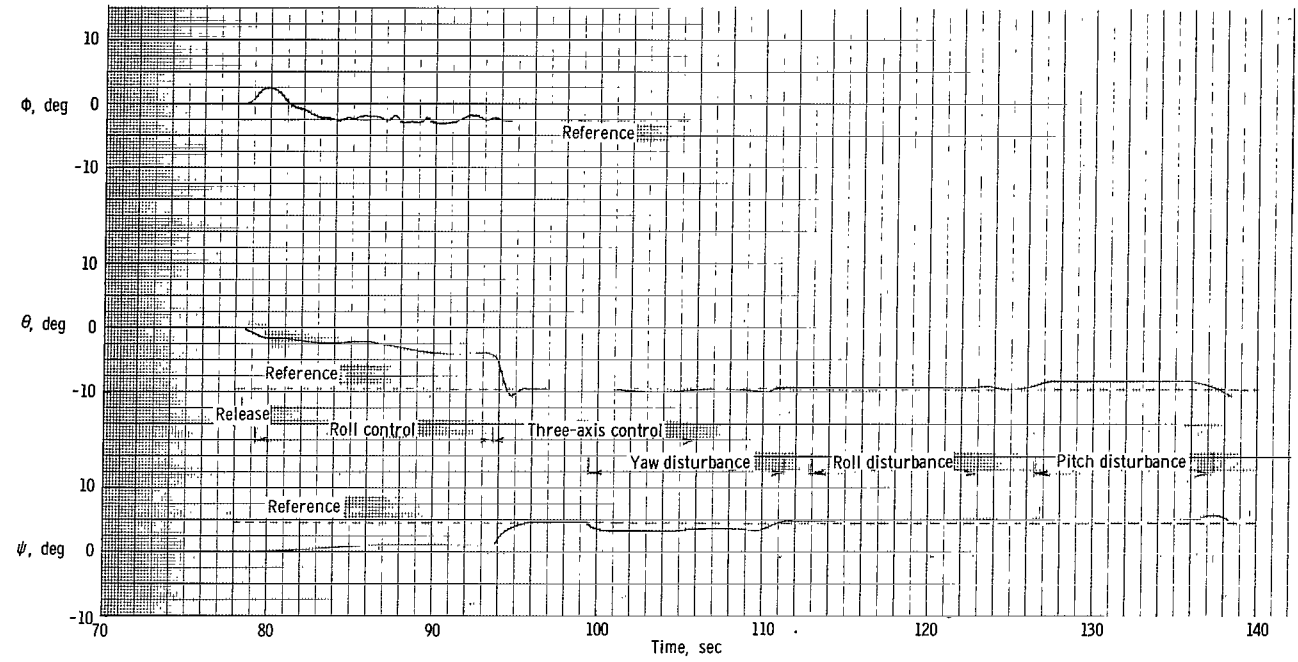

(a) Variation of ϕ, θ, and ψ with time.

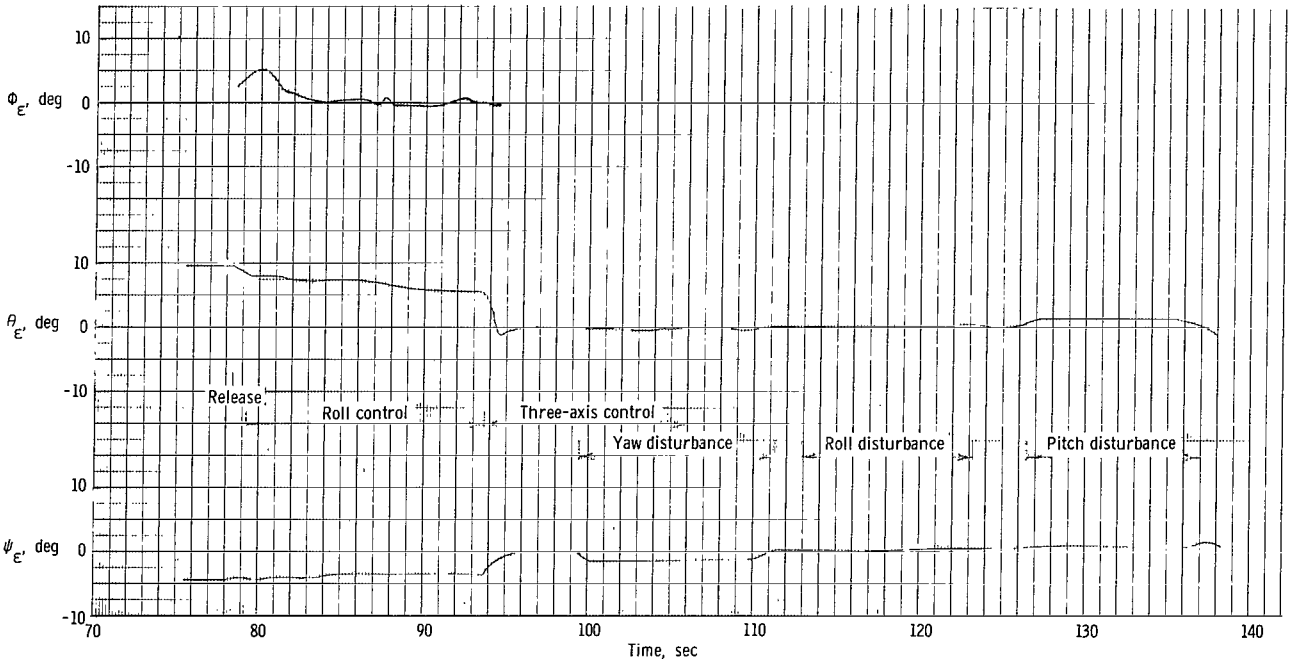

(b) Variation of $\phi_{\varepsilon'}$, $\theta_{\varepsilon'}$, and ψ_{ε} with time.

Figure 8.- Dynamic-test-stand investigation results obtained from camera data.

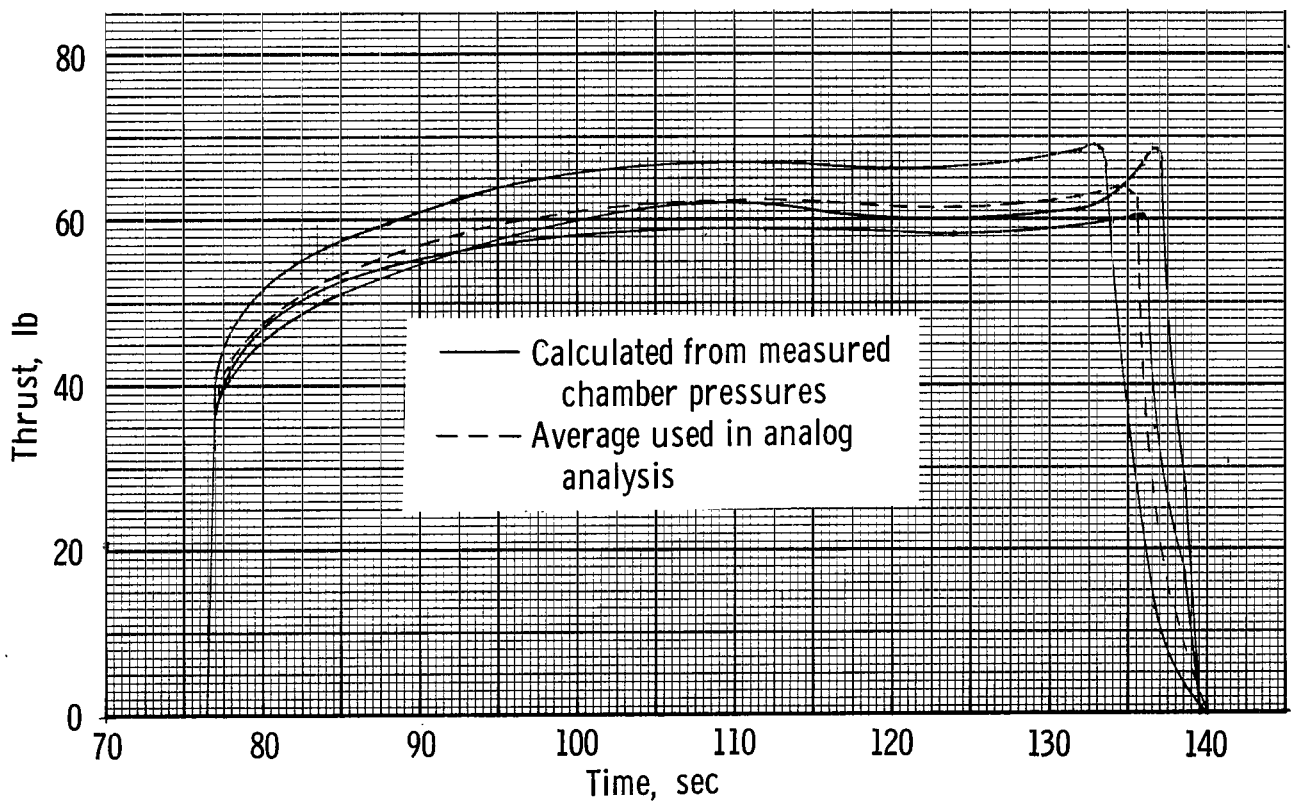

Figure 9.- Control-rocket thrust time histories.

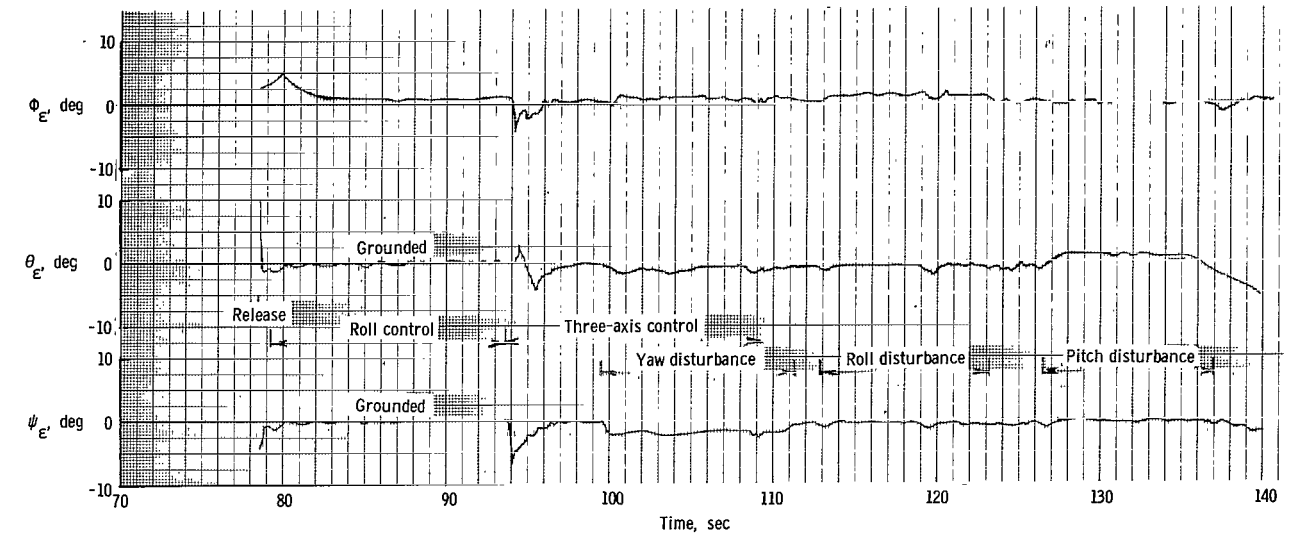

(a) Variation of ϕ_ε, θ_ε, and ψ_ε with time.

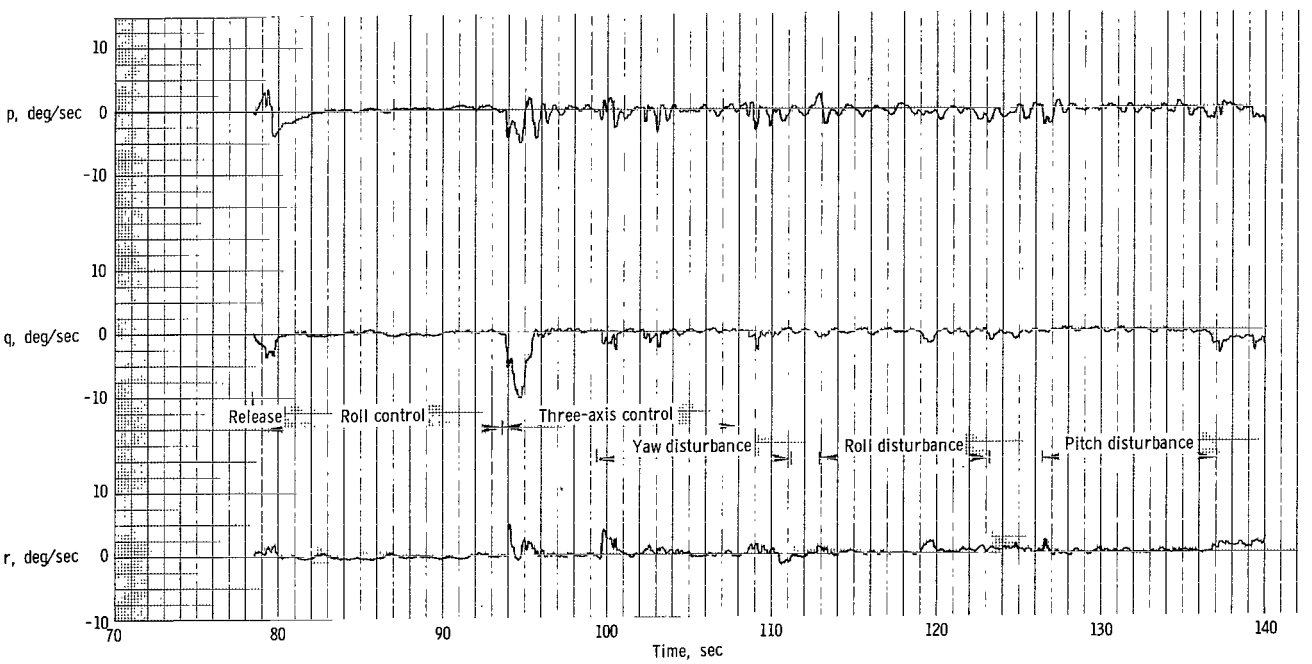

(b) Variation of p, q, and r with time.

Figure 10.- Dynamic-test-stand investigation results obtained from telemetry data.

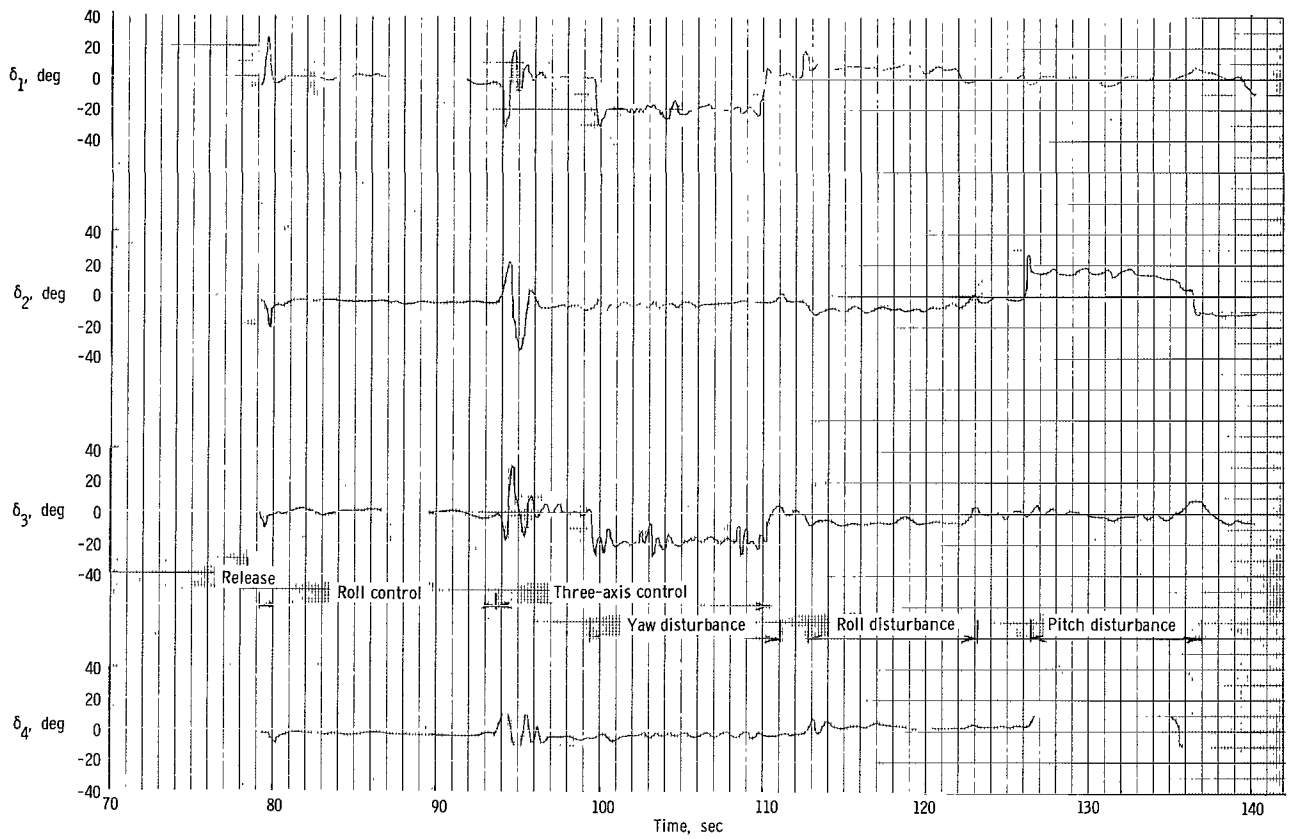

(c) Variation of δ_1, δ_2, δ_3, and δ_4 with time.

Figure 10.- Concluded.

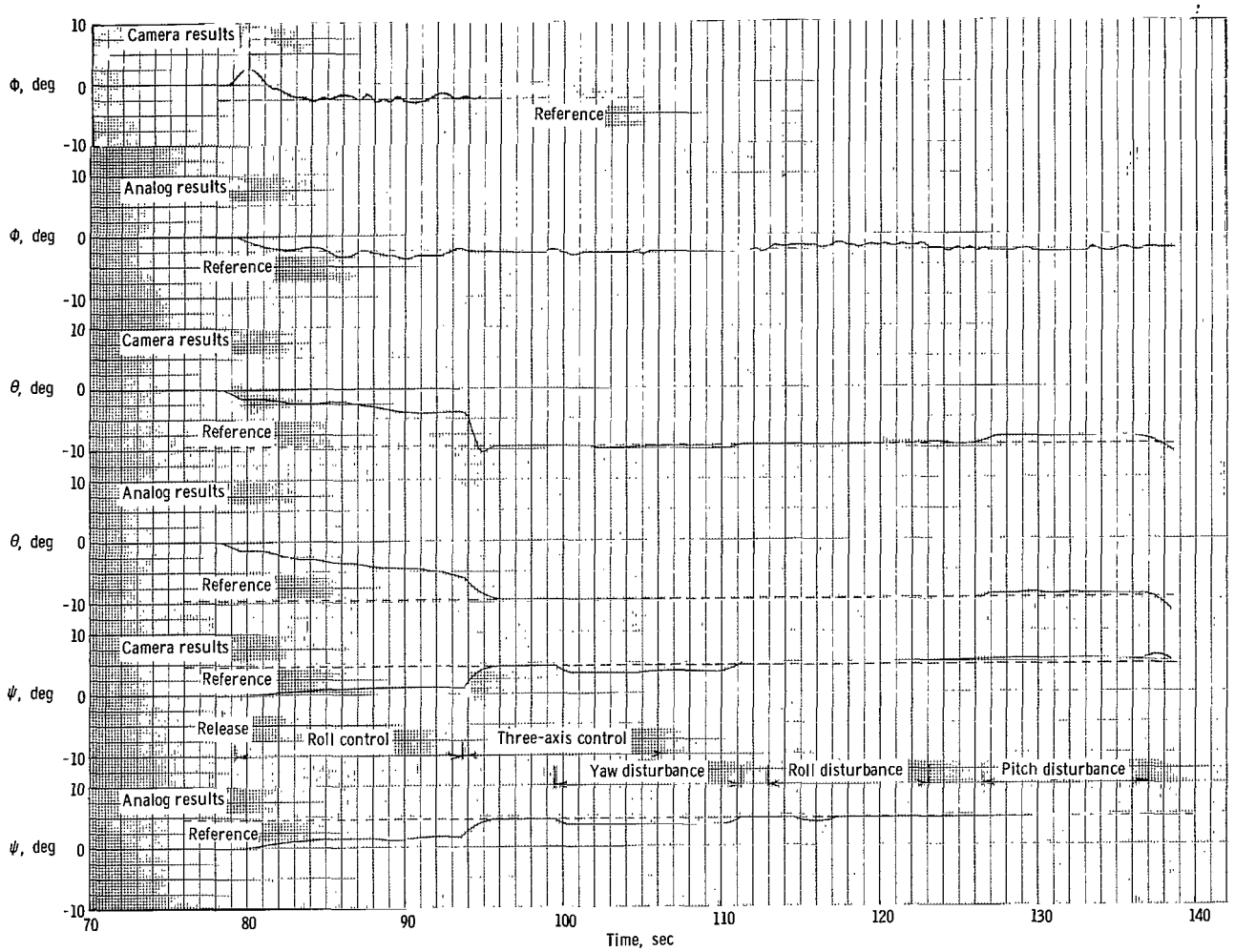

(a) Variation of ϕ, θ, and ψ with time.

Figure 11.- Comparison of analog simulation results and dynamic-test-stand investigation results.

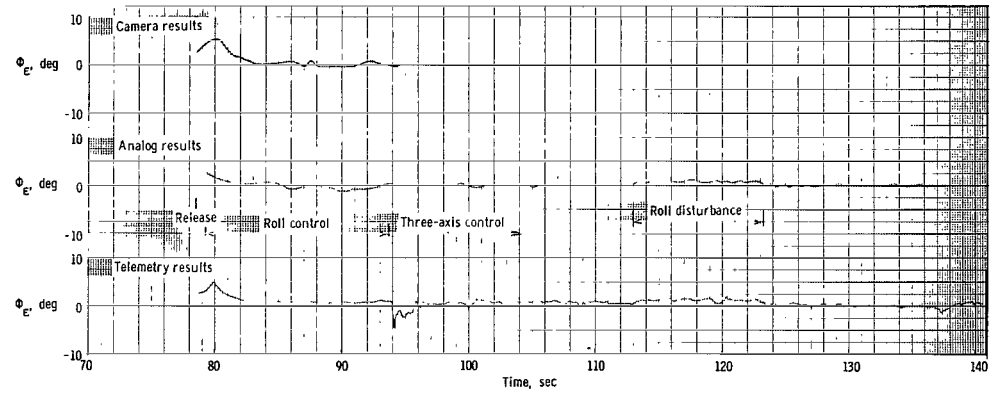

(b) Variation of ϕ_ε with time.

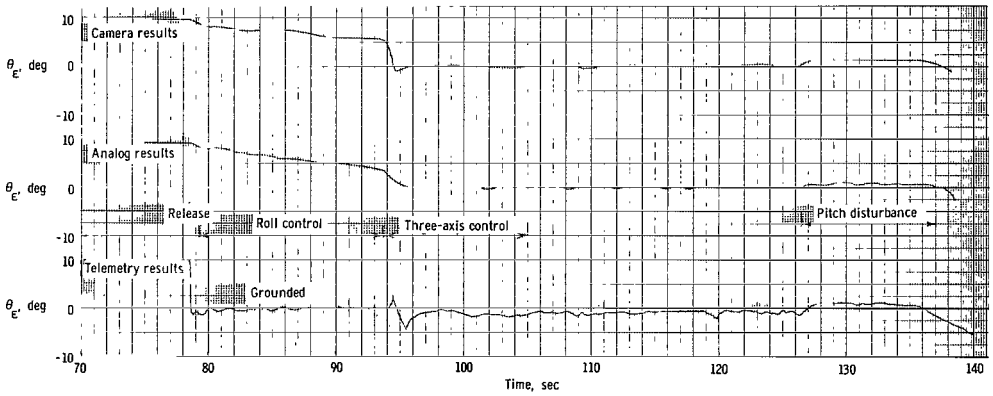

(c) Variation of θ_ε with time.

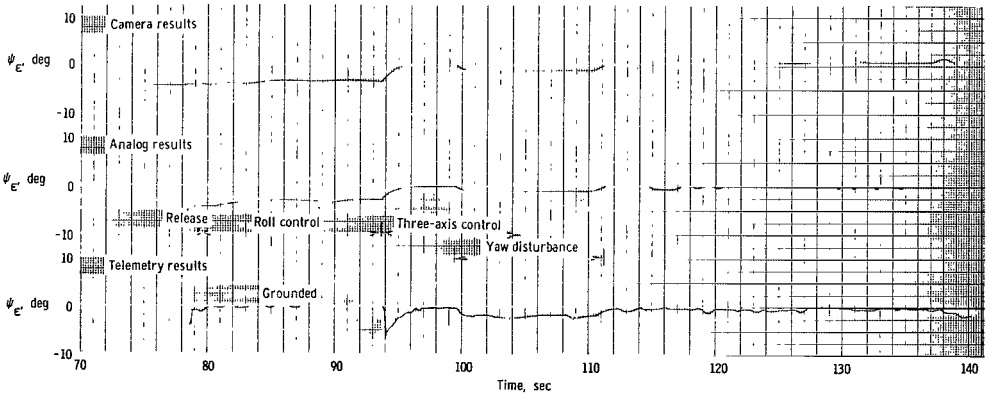

(d) Variation of ψ_ε with time.

Figure 11.- Continued.

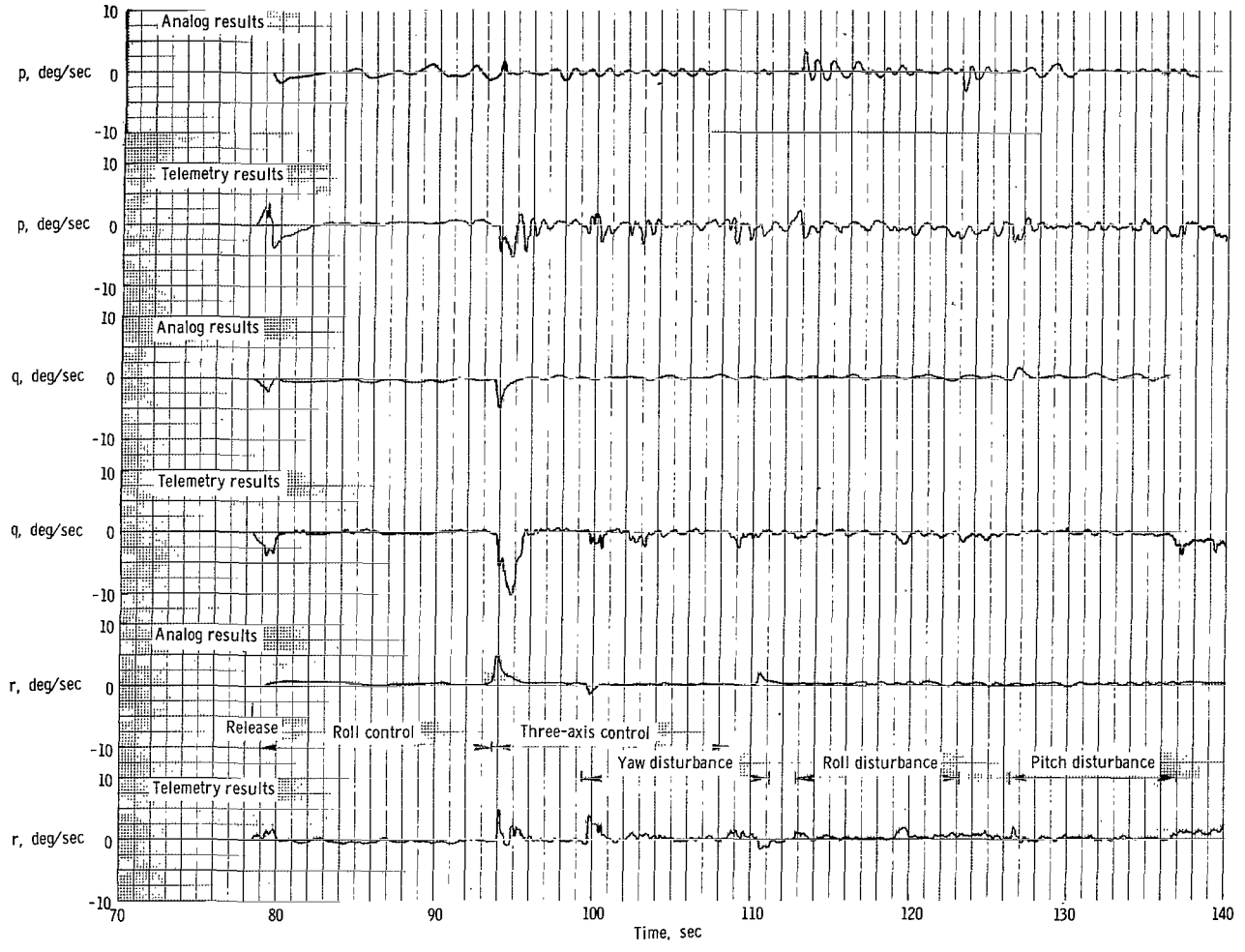

(e) Variation of p, q, and r with time.

Figure 11.- Continued.

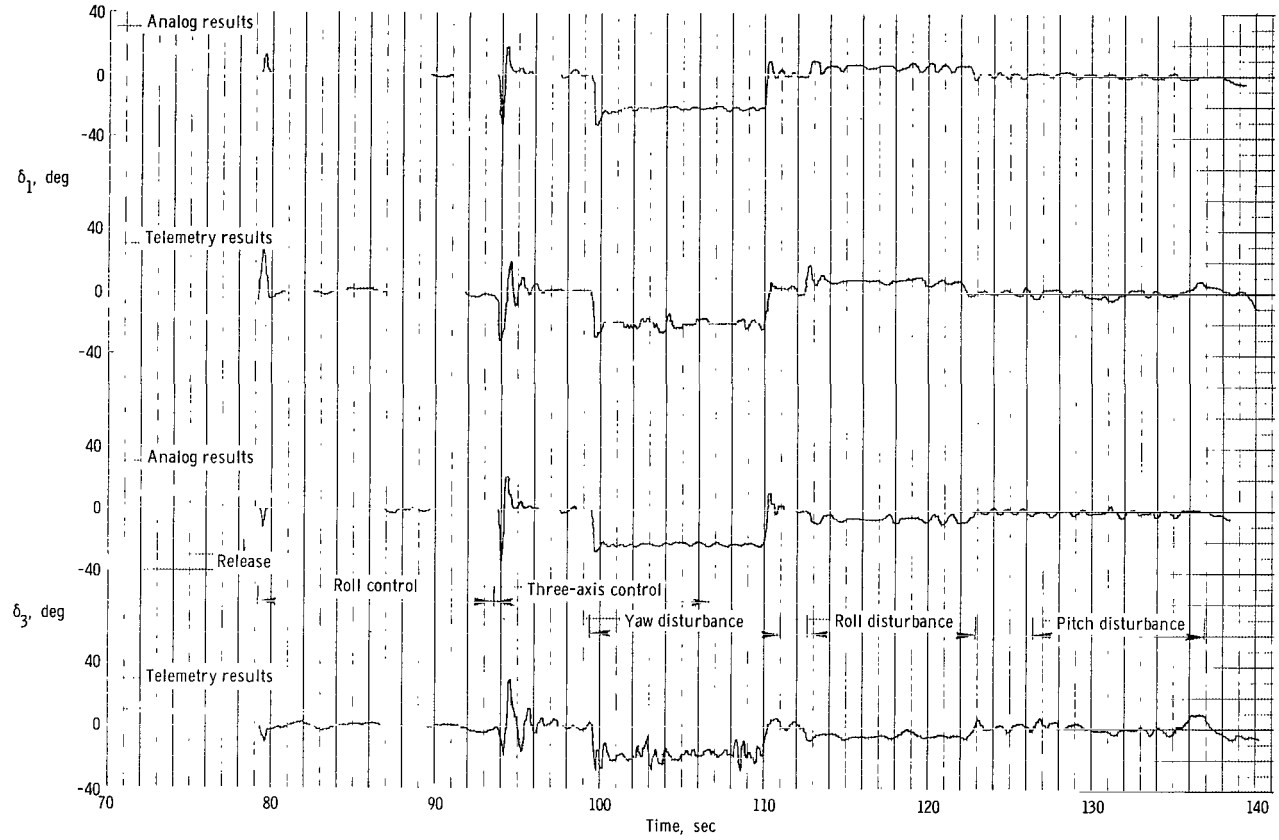

(f) Variation of δ_1 and δ_3 with time.

Figure 11.- Continued.

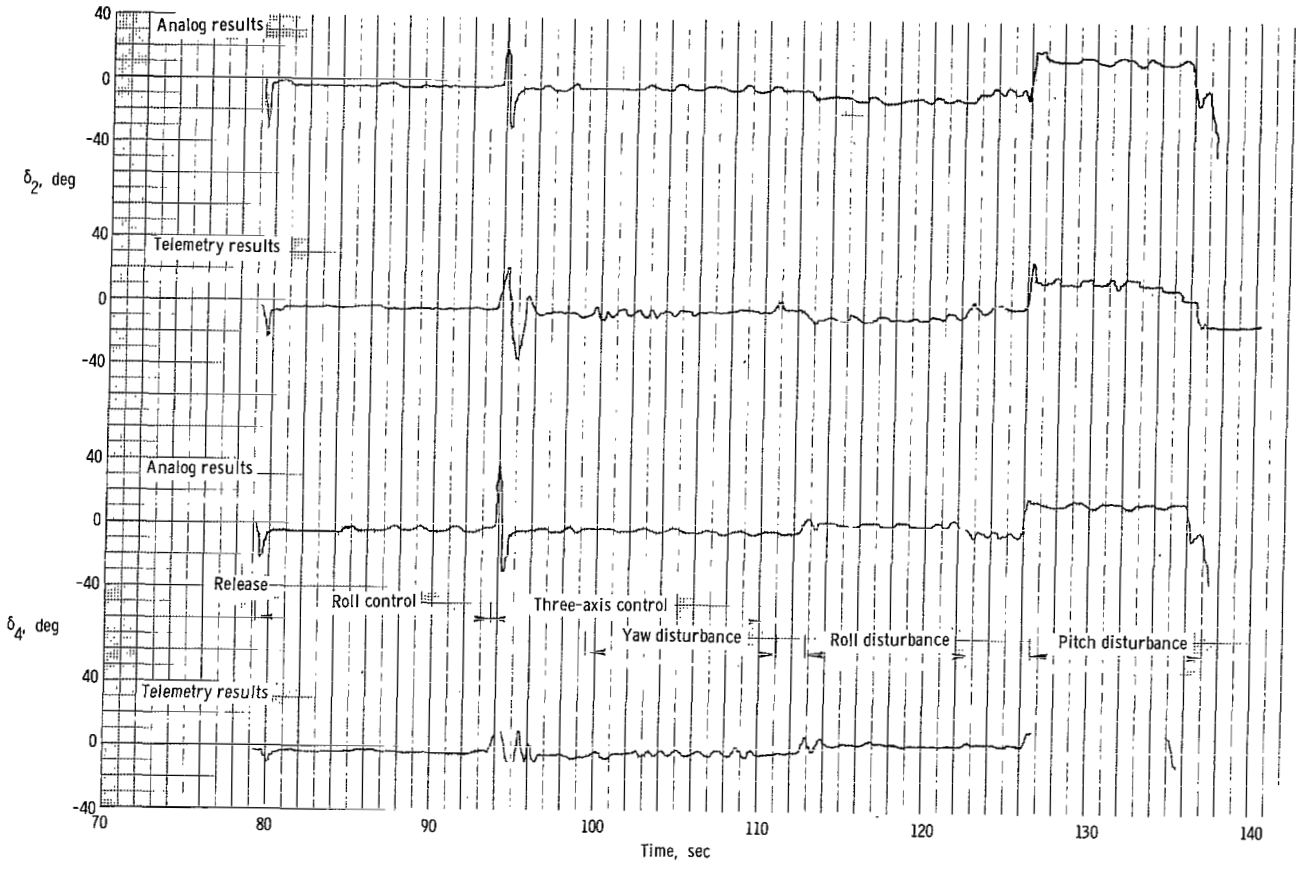

(g) Variation of δ_2 and δ_4 with time.

Figure 11.- Concluded.

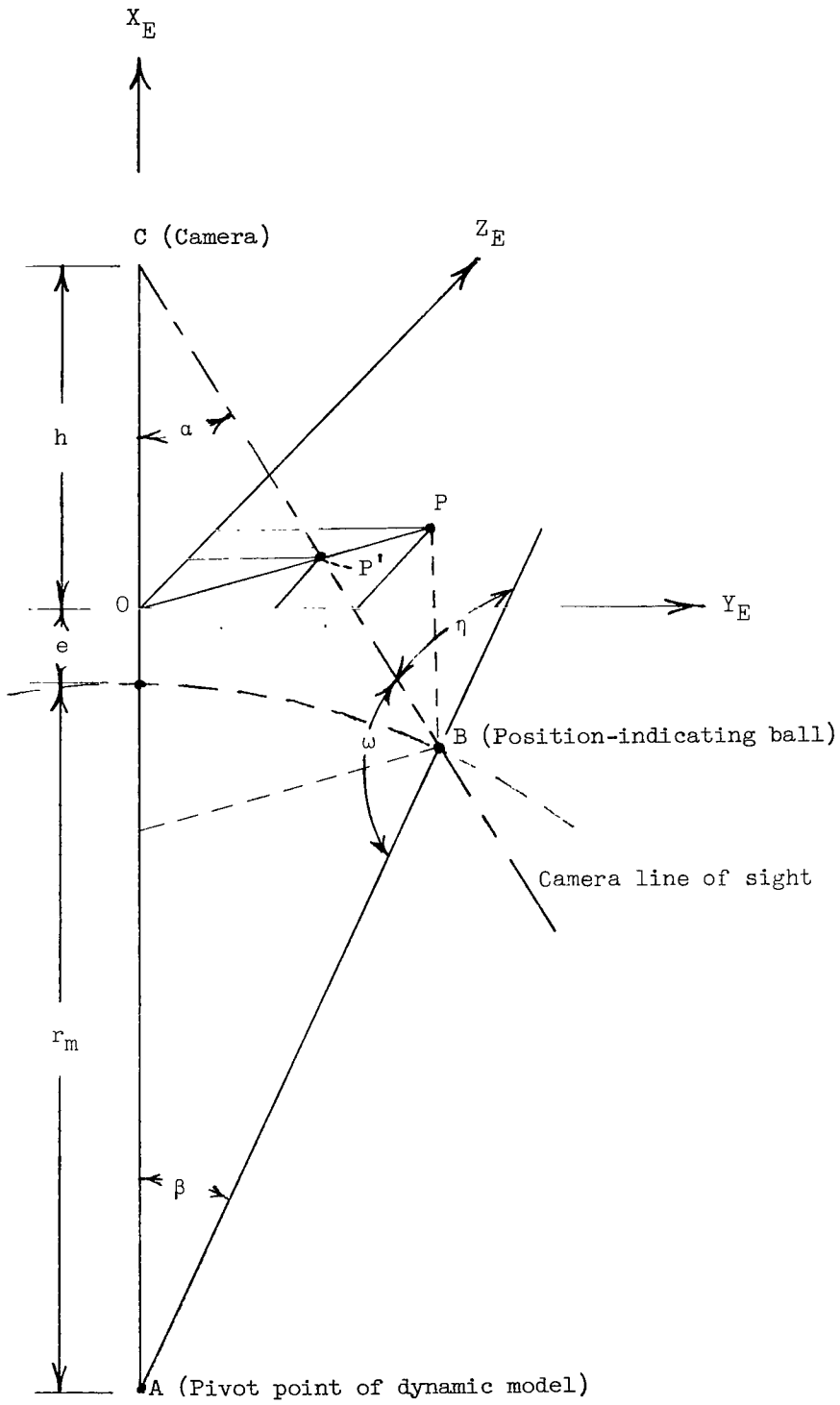

Figure 12.- Sketch used in derivation of equations for reducing camera data.

"The aeronautical and space activities of the United States shall be conducted so as to contribute . . . to the expansion of human knowledge of phenomena in the atmosphere and space. The Administration shall provide for the widest practicable and appropriate dissemination of information concerning its activities and the results thereof."

—NATIONAL AERONAUTICS AND SPACE ACT OF 1958

NASA SCIENTIFIC AND TECHNICAL PUBLICATIONS

TECHNICAL REPORTS: Scientific and technical information considered important, complete, and a lasting contribution to existing knowledge.

TECHNICAL NOTES: Information less broad in scope but nevertheless of importance as a contribution to existing knowledge.

TECHNICAL MEMORANDUMS: Information receiving limited distribution because of preliminary data, security classification, or other reasons.

CONTRACTOR REPORTS: Technical information generated in connection with a NASA contract or grant and released under NASA auspices.

TECHNICAL TRANSLATIONS: Information published in a foreign language considered to merit NASA distribution in English.

TECHNICAL REPRINTS: Information derived from NASA activities and initially published in the form of journal articles.

SPECIAL PUBLICATIONS: Information derived from or of value to NASA activities but not necessarily reporting the results of individual NASA-programmed scientific efforts. Publications include conference proceedings, monographs, data compilations, handbooks, sourcebooks, and special bibliographies.

Details on the availability of these publications may be obtained from:

SCIENTIFIC AND TECHNICAL INFORMATION DIVISION

NATIONAL AERONAUTICS AND SPACE ADMINISTRATION

Washington, D.C. 20546